Regional Studies in Marine Science
December 2023, Volume 67, Pages 103209 (17p.)
https://doi.org/10.1016/j.rsma.2023.103209 https://archimer.ifremer.fr/doc/00854/96592/

Influence of typology and management practices on water pCO and atmospheric CO2 fluxes over two temperate shelf – estuary – marsh water continuums

Mayen Jérémy [1, 2, *], Polsenaere Pierre [1], Regaudie De Gioux Aurore [3], Dupuy Christine [4], Vagner Marie [5], Lemesle Jean-Christophe [6], Poitevin Benoit [7], Souchu Philippe [2]

[1] IFREMER, Littoral, Laboratoire Environnement Ressources des Pertuis Charentais (LER/PC), BP 133, 17390, La Tremblade, France
[2] IFREMER, Littoral, Laboratoire Environnement Ressources Morbihan-Pays de Loire (LER/MPL), BP 21105, 44311, Nantes, France
[3] IFREMER, Dyneco, Pelagos, ZI de la Pointe du Diable - CS 10070, 29280 Plouzané, France
[4] UMR 7266 Littoral Environnement et Société (LIENSs), CNRS – La Rochelle Université, France
[5] LEMAR, UMR 6539 CNRS/Univ Brest/IRD/Ifremer, ZI pointe du diable, 29 280, Plouzané, France
[6] LPO, Réserve Naturelle de Lilleau des Niges, 17880, Les Portes en Ré, France
[7] Pôle-Nature de l'Ecomusée du Marais Salant, route de Loix, 17111, Loix en Ré, France

* Corresponding author : Jérémy Mayen, email address : jeremy.mayen@ifremer.fr

Abstract :

Within the coastal zone, salt marshes often behave as atmospheric CO2 sinks, allowing for blue carbon (C) sequestration associated with intense autotrophic metabolism. However, C dynamics over salt marshes are complex since various biogeochemical processes and fluxes occur at different terrestrial – aquatic – atmospheric exchange interfaces and spatiotemporal scales. This study focuses on seasonal, tidal and diurnal variations of water pCO 2, estimated water-air CO2 fluxes and controlling factors along two temperate shelf – estuary – marsh continuums. The latter include typical coastal systems with artificial salt marshes that have contrasting water management practices and primary producer types. Our high-frequency biogeochemical measurements (seasonal 24-hour cycles) highlighted a strong control of ecosystem typology on inorganic C dynamics with lower water pCO 2 values in the artificial salt marshes, due to stronger biological activity and longer water residence times, than in the tidal estuary. In the marine-dominated estuary, water pCO 2 variations (267 - 569 ppmv) were strongly controlled by tidal effects and phytoplankton activity particularly in spring/summer. On the contrary, the greatest amplitudes in water pCO 2 were recorded in the artificial salt marshes (6 - 721 ppmv) due to intense macrophyte activity. In the rewilded marsh, nutrient inputs favoured spring/summer fast-growing macroalgae produced, in turn, strong fall atmospheric CO2 outgassing from degraded algae waters and thus a net annual source of CO2 to the atmosphere (17.5 g C m−2 yr −1). Conversely, specific management practices at the working marsh for salt-farming activity favoured rather slow-growing macrophytes (i.e. seagrasses) which greatly contribute to the yearly observed atmospheric CO2 sink (-97.7 g C m−2 yr −1). In this work, we suggest that salt marsh management can be used to control the contribution of primary producers to marsh C budget as atmospheric CO2 (sink and/or source).

Graphical abstract

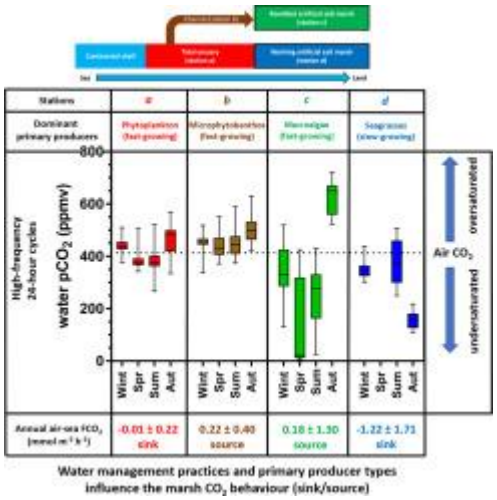

Water management practices and primary producer types influence the marsh CO_2 behaviour (sink/source)

Highlights

► Water pCO_2 variations exist along sea – land continuums according to station typology. ► Large pCO_2 amplitudes were recorded in artificial marshes at the diurnal/tidal scale. ► Water management practices in artificial salt marshes modulate their CO_2 behaviour. ► Fast-growing macroalgae in salt marshes produce a net atmospheric CO_2 degassing.

Keywords : shelf – estuary – marsh continuums, water pCO2, air-water CO2 fluxes, diurnal, tidal, seasonal scales, marsh management practices, macrophytes

1. Introduction

Marine coastal environments, which only account for 7% of the global ocean, perform major ecological functions such as primary production, bacterial mineralization and organic matter burial (Gattuso et al., 1998). The coastal zone presents a wide diversity of geomorphological types and ecosystems (shelves, estuaries, bays, wetlands) shaping the biogeochemical cycle coupling between land, ocean and atmosphere (Aufdenkampe et al., 2011; Bauer et al., 2013). These dynamics and heterogeneous ecosystems vertically exchanges large and variable quantities of carbon (C) with the atmosphere (Cole et al., 2007; Polsenaere et al., 2012). At the global scale, continental shelves behave as atmospheric CO_2 sinks and absorb 0.25 ± 0.05 Pg C yr^{-1} (Bauer et al., 2013; Dai et al., 2022) due to phytoplankton primary production (Cloern et al., 2014). On the contrary, CO_2 supersaturated estuarine waters emit 0.25 ± 0.05 Pg C yr^{-1} to the atmosphere (Bauer et al., 2013) due to a high mineralization of organic matter from the land (Frankignoulle et al., 1998; Borges and Abril, 2011). These atmospheric C exchanges within the coastal zone are heterogeneous (Borges et al., 2005) and need to be better taken into account in regional and global C budgets (Najjar et al., 2018). For instance, coastal wetlands, including salt marshes located along inner shelf – estuary – marsh continuums, absorb 0.55 ± 0.05 Pg C yr^{-1} from the atmosphere (Bauer et al., 2013) and may play a major role in atmospheric CO_2 uptake and associated organic C burial on Earth (Cai, 2011; Mcleod et al., 2011).

In salt marshes, inorganic C dynamics and water pCO_2 are influenced by several physicochemical and biological processes within and between each ecosystem compartment such as tidal exchanges, calcium carbonate precipitation/dissolution, benthic-pelagic coupling, air-water exchanges and photosynthesis/respiration balance (Cai, 2011; Bauer et al., 2013;

Macreadie et al., 2017). Due to high photoautotrophy rates of both aquatic (phytoplankton and macrophytes) and terrestrial (vascular plants) primary producers (Tobias and Neubauer, 2019), these highly productive ecosystems mostly behave as net atmospheric C sinks (Schäfer et al., 2014; Artigas et al., 2015; Forbrich and Giblin, 2015). A refractory part of organic C produced through photosynthesis in these vegetated coastal ecosystems can then be sequestered in sediments (Chmura et al., 2003) and stored as blue C, and greatly contribute to the regional/global C cycle in comparison with terrestrial ecosystems (Mcleod et al., 2011). Salt marshes also produce and horizontally export significant quantities of C through tidal water advection (Najjar et al., 2018) which could, in turn, strongly influence the C balance of the system itself as well as the estuary and shelf systems (Cai, 2011). The "marsh CO_2 pump" hypothesis proposes that atmospheric CO_2 fixation by plants and phytoplankton in marshes and the export of part of the associated C may be one of the major mechanisms making adjacent coastal waters sources of CO_2 to the atmosphere (Wang and Cai, 2004). For instance, in a tidal marsh area (USA; 12300 km^2), Wang et al. (2016) estimated that 56% (39% inorganic and 17% organic C forms) of its total net CO_2 fixation was exported to the coastal ocean. Nevertheless, despite these major ecological potentials (storm protection, nursery areas, long-term C storage), these interface areas are the most threatened in the world by land-use changes, climate changes and sea level rise (Gu et al., 2018). Moreover, coastal eutrophication causes the loss of salt marshes by decreasing the below-ground biomass of plant roots through microbial degradation thereby producing a decrease in the geomorphic stability of marshes (Deegan et al., 2012). Since the 1800s, salt marshes have lost about 25% of their global area with negative effects on the atmospheric CO_2 sink and the associated C sequestration (Mcleod et al., 2011). Their importance as ecosystem service reservoirs has made it possible to implement protection and

restoration policies that contribute to their better management and to the development of their ecological and economic potentials (Gu et al., 2018; Adam, 2019).

The high heterogeneity in biogeochemical processes within coastal systems at spatial and temporal scales (Cai, 2011; Bauer et al., 2013) requires more integrative C process and exchange measurements at the various terrestrial – aquatic – atmospheric interfaces over different time scales (tidal, diurnal and seasonal) to better understand the ecological functioning of these ecosystems facing global changes. Some studies in coastal wetlands such as salt marshes or tidal estuaries have taken water pCO_2 measurements at different temporal scales allowing the study of in situ CO_2 dynamics in relation to other biotic and abiotic processes. For instance, in an intertidal mangrove (Gaderu Creek, India), Borges (2003) showed a strong control of diurnal pCO_2 variations by tides and biological activity (primary production and respiration). However, still too few studies have taken high-frequency water pCO_2 measurements in salt marshes at the diurnal and tidal scales. These temporal variations in water pCO_2 strongly affect associated air-water CO_2 fluxes that can, in turn, be estimated from the CO_2 gas transfer velocity, CO_2 solubility in the water and air-water CO_2 gradient (Borges, 2003; Crosswell et al., 2017). The atmospheric Eddy Covariance technique represents an alternative way to directly measure atmospheric CO_2 fluxes at the ecosystem scale (Baldocchi et al., 1988; Schäfer et al., 2014). This non-intrusive micrometeorological technique allows to study the metabolism of coastal ecosystems (sink or source) under real field conditions and to integrate them into regional C budgets (Polsenaere et al., 2012; Van Dam et al., 2021).

The purpose of this study was to better understand CO_2 dynamics at different temporal scales and locations over two aquatic sea – land continuums along the Atlantic French coast on Ré Island. These continuums include coastal systems (shelf, estuary, marsh) such as those

studied elsewhere by Cai (2011) and Bauer et al. (2013) with regards to horizontal and vertical C exchanges in the coastal ocean. Unlike tidal salt marshes, which are more generally discussed in the literature (Wang et al., 2016), here we studied two artificial salt marshes (i.e. salt ponds) in which water exchanges are controlled by dykes and locks for human uses (biodiversity protection or anthropogenic activities). Through in situ high-frequency measurements of biogeochemical parameters in waters and estimations of atmospheric CO_2 fluxes from 2018 to 2020, we sought to (1) identify biophysical controlling factors of water pCO_2 by establishing biogeochemical relationships both at the seasonal and diurnal/tidal scales, (2) highlight the influence of continuum typologies on measured biogeochemical parameters and (3) identify role of station typologies and salt marsh management practices on temporal pCO_2 dynamics and associated CO_2 budgets. The results allowed us to contextualize the associated continuum metabolism among other studied systems from a C dynamic and budget point of view.

2. Materials and methods

2.1. Study sites

2.1.1. Tidal estuary (station *a*) and channel (station *b*)

The Fier d'Ars estuary is a semi-closed maritime area of 750 ha on Ré Island within the French Atlantic Ocean and connected to the Breton Sound continental shelf (Fig. 1). It corresponds to a type II temperate tidal estuary according to Dürr et al.'s (2011) coastal system typology. At low tide (LT), its subtidal zone (in light blue; Fig. 1) is composed of mudflats (slikke) and tidal salt marshes (schorre) traversed by numerous channels of different sizes. At high tide (HT), the subtidal zone is flooded by coastal waters from the shelf up to the dykes (Fig. 1), managed to control water exchanges between the estuary and upstream artificial salt

marshes. Station *a*, with a maximum water height of 6.5 m, is located within the subtidal zone of the estuary along the main channel connected to the slikke (Fig. 1). Station *b* is a secondary tidal channel associated to the schorre and located at the back of the estuary before the dyke. With a maximum water height of 5.3 m, it is connected to the station *a* (distance of 1.6 km) enabling the supply of coastal waters to artificial salt marshes upstream from the dyke (Fig. 1).

Artificial salt marshes are old tidal salt marshes divided into multiple ponds by dykes mainly located along European coasts for which water residence times (from a few hours to fifteen days according to the management practices; Bel Hassen, 2001) were originally controlled for salt-farming through locks (Tortajada et al., 2011).

2.1.2. Rewilded artificial salt marsh (station *c*)

Station *c* is a rewilded artificial salt marsh upstream from the dyke (surface area of 40100 m^2, depth of 60 cm), protected and managed inside a National Natural Reserve (NNR). During HT periods, this rewilded marsh is supplied indirectly with coastal waters from the estuary by the station *b* channel (distance of 500 m between stations *b* and *c*; Fig. 1) through a lock management practice to promote biodiversity protection (former salt farm that has been rewilded; Fig. A.1). From November until March (winter period), the marsh lock is open only during the highest tidal amplitudes in order to have the best compromise between salt- and fresh-mixing waters (salinity around 30) to allow aquatic fauna passing from the continental shelf to the marsh. From April to October (summer period) with lower tidal amplitudes, the lock is permanently open to avoid large salinity fluctuations and favour the development of *Ruppia spp.* seagrass beds in the marsh (salinity between 30 and 45). Lately, this rewilded marsh

is characterized by significant macroalgae development from early spring to late summer each year thereby preventing seagrass development (Champion et al., 2012).

2.1.3. Working artificial salt marsh (station *d*)

Station *d* is a working artificial salt marsh upstream from the dyke (surface area of 8500 m^2, depth of 75 cm) directly communicating (no channel in between) with coastal waters from the estuary through a lock (distance of 2 km between stations *a* and *d*; Fig. 1). This working marsh was chosen for its specific management practice of the lock related to a salt-farming activity. In spring and summer, the lock of is regularly open to store salt waters and then allow to supply upstream ponds succession during the neap tides for the salt production through the evaporation (Fig. A.1). Moreover, the use of this working marsh requires a drying up and a cleaning once a year in early spring before the start of the salt production period to remove seagrass, macroalgae and organic matter in the marsh (Poitevin, personal communication).

2.1.4. Additional station: continental shelf (station *F*)

The Breton Sound corresponds to a coastal maritime area located on the French continental shelf, characterized by a surface area of 425 km^2 (Fig. 1). The Breton Sound continental shelf exchanges salt waters with the Atlantic Ocean to the west at each semi-diurnal tidal cycle and receives continental inputs through the Aiguillon Bay discharges to the east depending on hydrodynamic and meteorological conditions (Stanisiere et al., 2006; Soletchnik et al., 2015). The highest and lowest river water flows were recorded in winter and summer, respectively, influencing salinity of the shelf waters differently. Station *F* in the centre of the Breton Sound

(Fig. 1) is located in a predominantly marine environment with a low freshwater contribution (Stanisiere et al., 2006; Soletchnik et al., 2015). At each HT, the continental shelf supplies our studied stations (*a*, *b*, *c* and *d*) with various water masses based on the tidal amplitudes and seasonal periods along two aquatic sea – land continuums: (1) continental shelf (station *F*) – estuary (station *a*) – channel (station *b*) – rewilded salt marsh (station *c*) and (2) continental shelf (station *F*) – estuary (station *a*) – working salt marsh (station *d*). Conversely, at each LT, different water masses from salt marshes are exported (indirectly through the station *b* channel for station *c* or directly for station *d*) to the estuary and then to continental shelf (Fig. 1).

In this study, meteorological parameters (air temperature, rain, wind speed) corresponding to our measurement cycles were used from the Eddy Covariance station (Campbell Scientific) deployed on a nearby tidal salt marsh (station *e*; Fig. 1).

2.2. Measurement strategy and biogeochemical measurements

In the subsurface water (~30 cm depth), partial pressure of CO_2 (pCO_2), temperature, salinity, turbidity, dissolved oxygen concentration (DO) and pH were autonomously measured with in situ probes at a frequency of 1 min. during fifteen 24-h cycles at stations *a*, *b*, *c* and *d* during each season (Table A.1). These high frequency measurements allowed to record relevant temporal (diurnal, tidal and seasonal) and spatial (continuums) variations of water pCO_2 and associated physicochemical parameters. The diurnal scale corresponds to fluctuations occurring between daytime and night-time whereas, the tidal scale corresponds to fluctuations between LT and HT. The seasonal measurement cycles were performed in 2018 at stations *a* and *b* and in 2019/2020 at stations *c* and *d*. Measurements could not be taken at station *d* in spring 2020

due to the Covid pandemic. At station *F*, the same biogeochemical measurements were taken biweekly over the year 2018 (Table A.1) by Coignot et al. (2020).

A pCO_2 underwater probe (C-Sense^{TM}; PME/Turner Designs), a multiparameter probe (EXO2; YSI) and a submersible fluorometer (C3^{TM}; Turner Designs) were deployed to measure water pCO_2, physicochemical parameters and fluorescence, respectively. The measurement range of the C-Sense probe is 0-2000 ppmv with an absolute accuracy of 60 ppmv (3% of the full scale; Turner Designs). The C-Sense probe was calibrated by the manufacturer before the study. The EXO2 probe was used to measure temperature (± 0.01 °C), salinity (± 0.5 salinity unit), turbidity (± 0.3 NTU), DO concentration (± 3.1 µmol L^{-1}), DO saturation level (± 1%) and pH (± 0.01 pH unit). The pH was calibrated before and after each 24-h cycle using three YSI buffer solutions (pH 4.01, pH 7.00 and pH 10.01) as outlined by Aminot and Kérouel (2004). It was not possible to measure pH at stations *a* and *b*. The C3-fluorometer was used to estimate the sub-surface Chl *a* values from the 10-min. fluorescence data. This latter was deployed only at station *c* and *d* in summer 2019 and winter 2020.

Water pCO_2 measured by the C-Sense probe are influenced by the total dissolved gas pressure (TDGP) which corresponds to the total pressure exhibited by all gases within the water column. When this pressure greatly exceeded the pressure at which the C-Sense probe was calibrated, the output needed to be corrected. Then, a pCO_2 correction was applied taking both TDGP, atmospheric pressure during sensor calibration (1009 hPa) and the measured pCO_2 by the C-Sense probe into account, as per equation ($pCO_{2measured}$ × 1009) / TDGP (Turner Designs). Over all 24-h cycles, the corrected pCO_2 values with TDGP were 2.6 ± 0.9% lower than the measured pCO_2 values. Total alkalinity (TA) and dissolved inorganic carbon (DIC) were estimated from salinity, temperature, pH and water pCO_2 using the carbonic acid constant from

Mehrbach et al. (1973) as modified by Dickson and Millero (1987), the K_{HSO4} constant from Dickson (1990) and the borate acidity constant from Lee et al. (2010). The CO_2 system calculation program (version 2.1.) performed these calculations (Lewis and Wallace, 1998).

2.3. Temperature and non-temperature effects on pCO_2 variations

To distinguish between the temperature and non-temperature effects on in situ pCO_2 variations at the seasonal and diurnal scales, $TpCO_2$ (pCO_2 variations related to temperature physical effects, in ppmv) and $NpCO_2$ (pCO_2 variations related to non-temperature effects, in ppmv) were calculated respectively, following (Eq. 1) and (Eq. 2) from Takahashi et al. (2002):

$$TpCO_2 = pCO_{2mean} \times \exp[0.0423 \times (T_{obs} - T_{mean})] \quad (1)$$

$$NpCO_2 = pCO_{2obs} \times \exp[0.0423 \times (T_{mean} - T_{obs})] \quad (2)$$

where T_{obs} and pCO_{2obs} are the temperature and pCO_2 values measured by the probes at each time step (1 min.), respectively. T_{mean} and pCO_{2mean} are the temperature and pCO_2 averaged either at the seasonal (annual mean) or diurnal scale (means per 24-h cycle). $TpCO_2$ is only associated with the physical pump whereas, $NpCO_2$ is associated with biological processes, tidal advection and benthic-pelagic coupling (Cotovicz Jr. et al., 2015; Polsenaere et al., 2022).

2.4. Calculations of air-water CO_2 fluxes

For all 24-h measurement cycles, the gas transfer velocity (k_{600}) and hourly CO_2 fluxes (FCO_2) at the air-water interface were estimated following Ribas-Ribas et al. (2011) and Polsenaere et al. (2022) in coastal environments. At stations *a* and *b*, only air-water FCO_2 during

HT periods (four hours around each HT) were calculated whereas at stations *c* and *d*, all hourly FCO_2 were calculated using the following formula (Eq. 3):

$$FCO_2 = \alpha \times k \times \Delta pCO_2 \quad (3)$$

where FCO_2 (mmol m^{-2} h^{-1}) is the estimated air-water CO_2 fluxes, α (mol kg^{-1} atm^{-1}) is the CO_2 solubility coefficient in saltwater, k (cm h^{-1}) is the gas transfer velocity of CO_2 and ΔpCO_2 (ppmv) is the gradient between mean water and air pCO_2. Water pCO_2 were measured by the C-Sense probe. Atmospheric CO_2 concentrations were measured by (1) the Eddy Covariance (station *e*; Fig. 1) for summer 2019 and winter 2020 and (2) the National Oceanic and Atmospheric Administration (NOAA) at the Mauna Loa Observatory for all other periods (see values caption Table 3). The α coefficient depends on water temperature and salinity and was calculated according to Weiss (1974). The *k* coefficient also significantly controls air-water FCO_2 since it directly takes turbulence processes at the air-water exchange interface into account (Polsenaere et al., 2013). In this study, *k* (or k_{660}) was calculated according to both Raymond and Cole (2001) (RC01; Eq. 4) and Wanninkhof et al. (2022) (W22; Eq. 5) corresponding to closed environments and more open coastal environments, respectively. These two parametrization methods for the *k* exchange coefficient were applied in order to compare the results.

For closed freshwater environments (Raymond and Cole, 2001):

$$k_{600} = 1.91 \times \exp[0.35 \times U_{10}] \quad (4)$$

For more open coastal environments (Wanninkhof et al., 2022):

$$k_{600} = 0.31 \times (U_{10})^2 \quad (5)$$

The gas transfer coefficients normalized to a Schmidt number of 600 (k_{600}) obtained with the two parametrization were then converted to the gas transfer velocity of CO_2 at the in situ temperature and salinity (k_{660}) according to Jähne et al. (1987) as per the equation (6):

$$k_{660} = k_{600} / (660/Sc)^{-0.5} \quad (6)$$

where k_{660} (cm h^{-1}) is the gas transfer velocity of CO_2 at the in situ temperature and salinity according to the parametrizations of RC01 or W22, U_{10} (m s^{-1}) is the wind speed normalized to 10 m (Amorocho and DeVries, 1980) and Sc is the Schmidt number which describes both the water viscosity and the molecular diffusion of the subsurface layer (Bade, 2009). In summer 2019 and winter 2020, wind speeds were measured by the Eddy Covariance (station *e;* Fig. 1) at a height of 3.15 m; for all other periods, wind data were obtained from the "Infoclimat" station (Fig. 1) measured at a height of 10 m (distances of 6.20, 4.85, 4.30 and 8.40 km from stations *a*, *b*, *c* and *d*, respectively).

2.5. Chl *a* concentrations and fluorometer data calibration

In situ Chl *a* concentrations (µg L^{-1}) were measured from sub-surface water samples collected only at stations *c* and *d*. Water samples (50-100 mL) were filtered through GF/F filters (Whatman® Nuclepore™, porosity of 0.7 µm) and stored at -20°C until analysis. In the dark, Chl *a* was extracted in 90% acetone with a glass rod. After 12 h of stirring at 4 °C to continue the extraction, Chl *a* was analysed by monochromatic spectrophotometry at 665 nm (Aminot and Kérouel, 2004).

For the fluorometer data, the calibration procedure was applied to derive Chl *a* values from our water fluorescence measurements (Aminot & Kérouel, 2004). Chl *a* could be calculated

only at station *d* through the significant linear regressions ($p < 0.05$) between the fluorometer values and the in situ Chl *a* values sampled simultaneously in the marsh waters.

2.6. Statistical tools and analysis

For all measured variables, the high-frequency data (i.e. 1 min) did not respect a normal distribution (Shapiro-Wilk tests, $p < 0.05$). Non-parametric comparison tests such as the Mann-Whitney and Kruskal-Wallis tests were carried out with 0.05 level of significance. A Dunn test was used to perform a post-hoc multiple comparison of the Kruskal-Wallis test to detect significant differences among groups. The statistical tests as well as temporal graphs, linear regressions, boxplot and barplot were performed with the GraphPad Prism 7 software. The R-studio software was used to perform the principal component analysis (PCA) with the FactoMineR package (Lê et al., 2008) and the correlation matrices with the corrplot package (Wei and Simko, 2017). The PCA allows to study the distribution of seasonal data along the studied continuums (Fig. 2). It is based on the seasonal means of the temperature, salinity, turbidity, DO and pCO_2 measured (i) once every two weeks at station *F* and (ii) once every minute over 24-h cycles at stations *a*, *b*, *c* and *d*. Stepwise multilinear regression analysis were performed to test the contribution of measured physicochemical variables (salinity, temperature, turbidity and oxygen) on water pCO_2 variations through the percentage of explained variance (adjusted R^2; Harrell, 2015). Within each measurement cycle, the selected multilinear model ($p < 0.001$, $n = 1441$) had the highest adjusted R^2 with all variables explaining at least 5% of the pCO_2 variation. Analysis were performed with Statgraphics Centurion 19 software.

3. Results

3.1. Biogeochemical overview of the aquatic continuums

Over our measurement periods, thermal conditions for the years 2018 and 2019 were similar following a classical seasonal trend. However, July 2018, July 2019 and February 2020 were warmer than the 1990-2020 reference period (Table 1). Annual cumulative precipitations in 2018 and 2019 were higher than the historical data with March 2018 and October 2019 as the rainiest months (Table 1). Salinity at station *F* as the water source flowing into the two continuums did not vary significantly between the years 2018, 2019, 2020 and the 2000-2017 reference period (Kruskal-Wallis test, $p = 0.77$; Fig. A.2).

At station *F*, over the biweekly measurements in 2018, water temperature varied from 7.5 (winter) to 21.7 °C (summer) whereas at station *a* over our seasonal 24-h cycles, values varied from 9.1 (winter) to 26.9 °C (summer). Along the aquatic continuum, the water temperature significantly increased from station *a* to stations *b* and *c* (Mann-Whitney tests, $p < 0.05$). Salinity ranged from 28.9 (winter) to 35.4 (autumn) at station *F*, whereas values varied from 31.4 (winter) to 35.7 (autumn) at station *a*, from 27.5 (winter) to 36.9 (autumn) at station *b*, from 27.0 (winter) to 42.6 (summer) at station *c* and from 21.3 (winter) to 38.4 (autumn) at station *d* with large salinity gradients at stations *c* and *d* (Table 2). In average over the year, the station *a* waters were slightly oversaturated in oxygen compared to the atmosphere with DO saturation levels ranging between 70 (LT during dawn) and 150% (LT during dusk) during the summer cycle (Fig. 3). The station *b* waters were close to the saturation value with the atmosphere with a lower maximum value (120%) during the summer cycle (Fig. 4). Larger amplitudes of DO saturation level were recorded in the artificial salt marshes with values ranging from 36 to 176% at station *c* (summer; Fig. 5) and from 49 to 150% at station *d*

(summer; Fig. 6). The annual levels of water CO_2 undersaturation with respect to the atmosphere were 48%, 16%, 65% and 86% at stations *a*, *b*, *c* and *d*, respectively, with a strong annual CO_2 oversaturation at station *b* (Fig. 4). The greatest amplitude in water pCO_2 was recorded at station *c* with values varying from 6 (spring) to 721 ppmv (autumn; Fig. 5).

At station *F*, over the year 2018, Chl *a* values increased from winter (0.7 ± 0.1 µg L^{-1}) to spring-summer (2.5 ± 1.6 and 1.6 ± 1.0 µg L^{-1}, respectively), before decreasing in autumn (0.8 ± 0.5 µg L^{-1}). At station *c*, the highest and lowest Chl *a* values were recorded in autumn 2019 (8.1 ± 0.4 µg L^{-1}) and winter 2020 (1.3 ± 0.3 µg L^{-1}), respectively whereas at station *d*, the highest and lowest values were recorded in winter 2020 (3.4 ± 0.4 µg L^{-1}) and summer 2019 (1.9 ± 0.3 µg L^{-1}), respectively. Moreover, at station *c*, from spring to autumn 2019, a free floating macroalgae development (*Ulva spp.*) was observed in the subsurface waters and on sediments (Fig. A.3). On the contrary, at station *d*, no macroalgae development occurred, allowing for the seagrass growth (*Ruppia spp.*) in the marsh (Fig. A.3).

3.2. Seasonal variations and controls along the aquatic continuums

Seasonally, the PCA reveals that stations along the aquatic continuums were vertically distinguished according to pCO_2, turbidity and DO saturation within PC2 explaining 35.5% of the total variance (Fig. 2). Within this axis, our results confirmed that water pCO_2 were seasonally negatively correlated with DO saturation ($r_{Pearson}$ = -0.56; n = 19; $p < 0.05$) and positively correlated with turbidity ($r_{Pearson}$ = 0.54; n = 19; $p < 0.05$) (Fig. 2). Station *b* recorded the highest water pCO_2 values and the lowest DO saturation levels compared to the three other studied stations (except in autumn; Table 2 and Fig. 2). Station *b* was also characterized by the highest turbidity values along the aquatic continuums (from 1.6 to 41 NTU). The PCA also

shows seasonal data were horizontally distinguished according to salinity and temperature within PC1 explaining 42.3% of the total variance (Fig. 2). Generally, the highest and lowest salinity values were recorded in summer and winter, respectively (Fig. 2), except at station *d* where the highest salinity were recorded in autumn (Table 2). At all studied stations, temperature and salinity values significantly varied between each seasonal 24-h cycles (Kruskall-Wallis tests, $p < 0.0001$).

Along the aquatic continuums, the PCA reveals contrasted seasonal variations of water pCO_2, particularly in artifical salt marshes (Fig. 2). At station *F*, in 2018, no significant difference in water pCO_2 were recorded at the seasonal scale (Kruskall-Wallis test, $p = 0.13$), although the highest and lowest seasonal means were recorded in winter and spring, respectively (Table 2 and Fig. 7). At station *a*, in 2018, water pCO_2 showed the same seasonal pattern decreasing from winter to summer before increasing in autumn, whereas station *b* showed lower seasonal variations over the same measurement periods (Table 2 and Fig. 7). In contrast, stations *c* and *d* showed larger seasonal pCO_2 variations (Fig. 7). Station *c* waters were undersaturated in CO_2 in spring 2019, summer 2019 and winter 2020 but oversaturated in autumn 2019 (622 ± 57 ppmv). At the same time, station *d* waters were undersaturated in CO_2 in summer, autumn and winter with the largest water CO_2 undersaturation recorded in autumn (155 ± 30 ppmv) in contrast to station *c* (Fig. 7). At all studied stations, water pCO_2 significantly differed between seasons (Kruskall-Wallis tests, $p < 0.05$), except for station *a* between spring and summer (Dunn's post-test, $p > 0.99$).

The same seasonal $NpCO_2$ variations were observed at stations *a* and *b* in 2018, with a decrease from winter (595 and 624 ppmv, respectively) to summer (296 and 347 ppmv, respectively) and an increase towards autumn (420 and 439 ppmv, respectively; Fig. 7). At

station *c*, the seasonal mean $NpCO_2$ value increased sharply from summer 2019 (193 ppmv) to autumn 2019 (630 ppmv) and then decreased towards winter 2020 (441 ppmv) whereas at station *d*, values slightly decreased from summer (286 ppmv) to autumn 2019 (160 ppmv) before increasing towards winter 2020 (453 ppmv; Fig. 7). Regarding temperature effects on water pCO_2, the highest and lowest seasonal $TpCO_2$ values were measured in summer and winter, respectively, with seasonal $TpCO_2$ values followed systematically by seasonal water temperature variations (Fig. 7). At station *a*, $\Delta TpCO_2$ offset recorded from winter to summer 2018 ($\Delta TpCO_2$ = 240 ppmv, from 310 to 550 ppmv) concomitantly to the water temperature increase of 13.4 °C partly compensated non-thermal effects on water pCO_2 during this period ($\Delta NpCO_2$ = 299 ppmv, from 595 to 296 ppmv).

3.3. Diurnal/tidal variations and controls along the aquatic continuums

At stations *a* and *b* in winter, salinity varied at the tidal scale with the lowest values at LT and the highest values at HT whereas from spring to autumn, the opposite pattern was recorded with salinity decreases at each incoming tide from the shelf (Figs. 3 and 4). At stations *c* and *d*, even stronger salinity gradients were recorded, especially in summer with decreases of 9 and 5 salinity units, respectively (Figs. 5 and 6). At station *c*, coastal water inflows led to an increase in salinity only in winter (Fig. 5). At station *d*, salinity and turbidity did not vary neither in autumn or in winter (Fig. 6).

The largest diurnal/tidal variations in the water pCO_2 and DO concentrations occurred during summer with pCO_2 ranges of 255, 216, 405 and 258 ppmv at stations *a*, *b*, *c* and *d*, respectively, and DO ranges of 153.2, 152.2, 262.8 and 205.6 µmol L^{-1} at stations *a*, *b*, *c* and *d*, respectively. At stations *a* and *b* , the low tide periods during the day (LT/D) occurring at dawn

showed higher water pCO_2 values and lower DO saturation levels than the low tide periods during the night (LT/N) occurring at dusk under similar salinity ranges, particularly in summer (Figs. 3 and 4). In general, our diurnal cycles showed a pCO_2 decrease that was negatively correlated to a DO increase during daytime (except at station *c* in spring; Fig. 5) and an opposite pattern during night-time (except at station *c* in summer; Fig. 5). At station *c*, in winter during the LT periods (no salinity variation), water pCO_2 decreased of 390 ppmv during the day (from 09:00 to 17:00) and increased of 230 ppmv during the night (from 20:00 to 05:00), while DO increased of 76.6 µmol L^{-1} and decreased of 29.0 µmol L^{-1}, respectively (Fig. 5). At station *d*, the same diurnal water pCO_2 and DO patterns were recorded at each 24-h cycle (Fig. 6). However, these strong diurnal pCO_2 and DO variations were significantly disrupted once coastal water advection and marsh management practices occurred.

Strong tidal variations in water pCO_2 were recorded during all seasonal cycles except at station *d* both in autumn and winter (Fig. 6). At stations *a* and *b*, incoming tides from the shelf during the day produced rapid water pCO_2 decreases from an oversaturation to a slight water undersaturation, particularly in spring (-121 and -167 ppmv, respectively) and summer (-139 and -115 ppmv, respectively; Figs. 3 and 4). Only at station *a*, ebbing tides during the day generated an additional pCO_2 decrease to reach the lowest values (Fig. 3). At station *a*, in summer and autumn and at station *b* over the four seasons, incoming tides during the night produced pCO_2 increases leading to water oversaturation periods (Figs. 3 and 4). Along the continuum, at station *c* during the night, higher water pCO_2 values were recorded at HT than at LT, especially in spring (363 ± 85 and 16 ± 5 ppmv at HT/N and LT/N, respectively) and in winter (431 ± 6 and 323 ± 53 ppmv at HT/N and LT/N, respectively; Fig. 8). The same tidal pCO_2 pattern was also recorded at station *c* in summer during the day (323 ± 88 and 197 ± 141 ppmv at HT/D and LT/D, respectively; Fig. 8). In spring, the station *c* marsh recorded lowest

water pCO_2 values both the day and the night during the marsh confinement but coastal water inflows from the station *b* channel instantly produced a large and rapid increase in water pCO_2 (+395 ppmv) mostly within a two-hour period (Fig. 8).

For all 24-h cycles, strong and significant correlations between pCO_2 and $NpCO_2$ were computed (Figs. 3-6). Similarly, water pCO_2 values were negatively correlated with DO saturation levels at 24-h cycles ($n = 1441$, $p < 0.05$), with $r_{Spearman}$ ranging from -0.67 (winter) to -0.97 (autumn) at station *a*, from -0.63 (summer) to -0.87 (autumn) at station *b*, from -0.54 (winter) to -0.86 (autumn) at station *c* and from -0.59 (winter) to -0.80 (autumn) at station *d*. At station *d*, negative correlations were obtained between measured pCO_2 and estimated Chl *a* in summer ($r_{Spearman} = -0.44$; $n = 105$; $p < 0.05$) and in winter ($r_{Spearman} = -0.60$; $n = 144$; $p < 0.05$) (Fig. 6). At station *a*, in winter, the multilinear regression analyses highlighted that water pCO_2 were controlled by DO, temperature and salinity whereas over other seasons, pCO_2 were strongly controlled only by DO with the highest R^2 values (Table 4). At station *a*, in spring and summer, estimated TA values were weakly correlated with measured pCO_2 and pH values (Fig. A.4) whereas in autumn, stronger correlations TA versus pCO_2 were recorded ($R^2 = 0.89$ and $R^2 = 0.71$, respectively; $n = 1441$; $p < 0.05$). At station *c*, water pCO_2 were mainly controlled by both salinity and DO in spring, by salinity in summer and by DO in autumn (Table 4). Finally, at station *d*, pCO_2 were mostly explained by salinity and DO in summer (salt farming period) and by DO and temperature in autumn/winter (marsh confinement periods) (Table 4).

3.4. Air-water CO_2 flux variations

Mean air-water CO_2 fluxes (FCO_2) according to the W22 parametrization were estimated to be -0.01 ± 0.22, 0.22 ± 0.40, 0.18 ± 1.37 and -1.22 ± 1.71 mmol m^{-2} h^{-1} at stations

a (sink), *b* (source), *c* (source) and *d* (sink), respectively, whereas station *F* waters behaved as a CO_2 source (0.30 ± 1.04 mmol m^{-2} h^{-1}). Large seasonal and diurnal variations were observed at the studied stations (Fig. 9). On average, station *a* showed positive FCO_2 values in both winter and autumn (slight CO_2 source) but negative means in spring and summer (slight CO_2 sink; Table 3 and Fig. 9). At station *b*, positive FCO_2 values were estimated, with maximum and minimum FCO_2 mean values occurring in winter and summer, respectively (Table 3 and Fig. 9). Station *c* behaved as a CO_2 sink in spring, summer and winter and as a strong CO_2 source in autumn (Table 3). At this marsh station, FCO_2 varied between -3.00 and 0.03 mmol m^{-2} h^{-1} in spring and between 0.61 and 4.61 mmol m^{-2} h^{-1} in autumn (Fig. 9). Station *d* behaved as a CO_2 sink in summer, autumn and winter with the largest atmospheric CO_2 uptake in autumn (Table 3) where FCO_2 varied between -6.03 and -1.79 mmol m^{-2} h^{-1} (Fig. 9).

4. Discussion

4.1. Biogeochemical parameter relationships and pCO_2 controls along the shelf - estuary - marsh continuums

At the tidal estuary (*a*) and its associated channel (*b*), seasonal non-thermal effects (biological and tidal affects) inducing heterotrophy in winter and autotrophy in summer were offset by thermal effects and resulted in low seasonal variations of water pCO_2 (Fig. 7). Similar observations were reported in two marine-dominated estuaries (Jiang et al., 2008) and in the Arcachon coastal lagoon (Polsenaere et al., 2022). In the estuarine waters here, thermal effects decreased and increased in situ pCO_2 values of 30 and 40% in winter and summer, respectively. On the contrary, at the rewilded marsh (*c*), seasonal water pCO_2 were strongly controlled by non-thermal effects promoting autotrophy both in spring and summer and heterotrophy in

autumn, mostly due to macroalgae activity whereas at the working marsh (*d*), thermal effects in summer and biological effects in autumn strongly controlled seasonal water pCO_2 (Fig. 7).

At the diurnal scale, the biological influence on continuum water pCO_2 dynamics through autotrophic and heterotrophic processes was significant at each station as endorsed by strong linear relationships between pCO_2 and DO, especially in autumn (Table 4). At the tidal estuary (*a*), from spring to autumn, diurnal pCO_2 variations were mostly controlled by the photosynthesis versus respiration balance of planktonic communities; indeed, more than 80% of the pCO_2 variance was modelled with DO only (Table 4). Dai et al. (2009) highlighted that CO_2 biogeochemical processes in coastal environments such as our estuary are generally controlled by non-thermal effects, like biological activity, compared to more open systems. Several studies have shown a major biological control on diurnal pCO_2 variations in coastal systems such as the temperate Bay of Brest (France; Bozec et al., 2011), the temperate Arcachon lagoon (France; Polsenaere et al., 2022), the shallow subtropical estuary in Tampa Bay (USA; Yates et al., 2007) and the tropical coastal embayment at Guanabara Bay (Brazil; Cotovicz Jr. et al., 2015). At the rewilded marsh (*c*), while in spring and summer, the high primary production of macroalgae induced large periods of water CO_2 undersaturation with respect to the atmosphere, winter pCO_2 variations were rather induced by planktonic community activity (ciliates > 2 10^4 cell L^{-1}; unpublish result). At the working marsh (*d*), the negative correlations between pCO_2 and Chl *a* associated with strong non-thermal contributions ($\Delta NpCO_2$ = 318 ppmv in summer for instance) showed a major biological influence on diurnal pCO_2 variations as well. By comparison, in a *Zostera marina* meadow (South Bay, USA), Berg et al. (2019) measured similar diurnal fluctuations of water pCO_2 that were directly controlled by seagrass metabolism with diurnal ranges of 528 and 603 ppmv in spring and summer, respectively.

Tidal advection between continental shelf and salt marshes also significantly controlled water pCO_2 dynamics and associated station biogeochemical status. This control was supported by the linear relationships between water pCO_2 and salinity as observed at each station from winter to summer whereas, relationships with turbidity were rather related to the hydrodynamic forcing on water pCO_2 (Table 4). At the tidal estuary (*a*) and its associated channel (*b*), daytime incoming tides created a significant decrease in water pCO_2 since the advected shelf waters were CO_2 undersaturated with respect to the atmosphere contrary to estuarine waters. In the Arcachon lagoon, seasonal measurement cycles also showed a strong tidal control on inorganic C parameters with lower pCO_2 values measured at high tide than at low tide irrespective of day or night status (Polsenaere et al., 2022). Even stronger tidal influences on water pCO_2 (from 1380 to 4770 ppmv) were observed during a summer cycle in the Gaderu Creek mangrove (Borges, 2003). In summer, the large pCO_2 decrease in the studied estuarine waters at ebbing tide the day, associated with strong DO saturation level increase was probably due to CO_2 undersaturated water exports from the productive salt marshes upstream. Indeed, in spring and summer, the rewilded marsh waters (*c*) were CO_2 depleted due to strong autotrophy activity. Conversely, more CO_2-enriched coastal water inflows from the shelf and the estuary into the marsh instantly produced significant salinity decreases and pCO_2 increases (Table 4). Therefore, at each semi-diurnal tidal cycle, horizontal advection had significant effects on water pCO_2 dynamics (except during marsh confinement) but variations strongly depended on the biogeochemical state of advected waters from upstream/downstream and the ecosystem typology (estuary, marsh, channel).

4.2. Continuum typologies revealed from measured biogeochemical parameters

In the coastal ocean, a strong influence of ecosystem typology (continental shelf, estuary, marsh) on biogeochemistry is generally observed and particularly, on inorganic C (Bauer et al., 2013). In our study, in 2018, watershed-influenced shelf waters (*F*) were characterized by lower salinity values than the Atlantic Ocean (35.6; Vandermeirsch 2012), confirmed over the 2000-2017 reference period (Belin et al., 2021). However, shelf waters showed a rather weak influence of terrestrial inputs on water pCO_2 dynamics (annual non-significant salinity and pCO_2 relationship, $p = 0.88$). At this shelf station, phytoplankton bloom with centric diatoms generally occurs in spring and summer (Guarini et al., 2004) and can induce water CO_2 undersaturation as also observed on the Belgian continental shelf (Borges and Frankignoulle, 1999). Along the continuum, the tidal estuary (*a*) influenced by buffered shelf waters was CO_2 undersaturated at 4% in winter and 82% in spring/summer that could be attributed to coastal water autotrophic activity at this period. Previous study carried out in the same estuarine waters measured Chl *a* concentrations from 0.2 (winter) to 3.5 µg L^{-1} (spring/summer) and a Chl *a* export suggesting a net primary production within this tidal estuary (Bel Hassen, 2001). Additionally, Savelli et al. (2019) observed in a nearby intertidal zone that microphytobenthos (MPB) may also contribute to estuarine water CO_2 undersaturation and to the overall water column Chl *a* concentration through tidal resuspension. Due to the small insulary catchement area (1200 ha) consisting only of salt marshes (no terrestrial water input), the CO_2 dynamics in the tidal estuary (*a*) is different from other estuaries worldwide (Borges and Abril, 2011). Similarly, the marine-dominated estuary of Sapelo Sound (USA) was also characterized by lower water pCO_2 values than river-dominated ones (Borges and Abril, 2011) but bacterial remineralization of organic carbon produced by *Spartina* in nearby salt marshes strongly increased water pCO_2 in summer (Jiang et al., 2008) contrarily to our studied estuary.

Overall, channel (*b*) waters between the estuary and salt marshes showed the longest periods of CO_2 oversaturation with respect to the atmosphere. At this channel, strong hydrodynamic forcings during incoming and ebbing tides produced more turbid waters due to organic matter resuspension from muds (Guarini et al., 2008). It probably limited the primary production (phytoplankton, MPB) by low light availability in water column (Cloern, 1987) and, on the contrary, favoured heterotrophic processes (Polsenaere et al., 2022). In channel waters, we recorded lower DO concentrations (-10%) and higher pCO_2 values (+10%) than in estuarine waters under similar salinity ranges. In channel waters at the same location, Tortajada (2011) measured POC/Chl *a* > 200 mg mg^{-1} throughout the year and even POC/Chl *a* > 600 mg mg^{-1} in autumn. This detrital/heterotrophic material may indicate microbial mineralization processes from MPB and confirm the water CO_2 oversaturation periods. However, channel (*b*) waters showed lower pCO_2 values than those from other coastal channel systems probably due to low terrestrial water inputs upstream/downstream over the estuary. The Sancti Petri Channel waters and its nearby salt marshes between the Atlantic Ocean and the Cadiz Bay (Spain) were also mainly CO_2 oversaturated (281 - 862 ppmv), due to DIC inputs from diagenetic processes of organic matter in mudflats that constitute a CO_2 source to water column (Burgos et al., 2018). Indeed, within the Duplin River salt marsh-estuary coastal system (USA), higher summer pCO_2 and DIC values were recorded at low tide in channel waters (12000 ppmv and 4300 µmol L^{-1}, respectively) than at high tide in marsh waters (1600 ppmv and 2200 µmol L^{-1}, respectively; Wang et al., 2018).

Contrary to estuarine and channel waters, artificial salt marshes (*c* and *d*) waters were characterized by the lowest turbidity and highest salinity values due to longer water residence times. These lower hydrodynamic conditions promoted the development of primary producers and as a result, biological CO_2 uptake associated with the highest DO saturation levels. In turn,

the salt marshes showed lower water pCO_2 values and longer water CO_2 undersaturation periods mainly due to a strong macrophyte activity (macroalgae at rewilded marsh and seagrasses at working marsh) than the tidal estuary and elsewhere similar wetland typologies (Borges, 2003; Burgos et al., 2018; Wang et al., 2018; Berg et al., 2019). Unlike seagrasses which are known to be important blue C systems (Mcleod et al., 2011), macroalgae developing in coastal wetlands have a limited capacity to store C over the long-term. However, studies have shown their potential contribution to coastal blue C by (i) storing large organic matter quantities in their living biomass through their high primary production (Raven, 2018) and (ii) transferring it to adjacent systems through tides and storage in coastal sediments (Duarte and Cebrián, 1996; Hill et al., 2015; Krause-Jensen and Duarte, 2016). Our pCO_2 observations are in accordance with these reports with the role of C storage by macrophytes in these shallow salt marshes.

4.3. Temporal carbon modulation by management practices

Management practices at the artificial salt marshes correspond to specific water lock actions linked to anthropogenic activities. They can strongly modulate water fluxes from the estuary and thereby influence marsh pCO_2 dynamics. At the rewilded marsh (*c*), the specific management practice by the NNR produced favourable conditions for free floating macroalgae development from early spring to late summer under low water marsh hydrodynamic and high air and water temperature conditions (Newton and Thornber, 2013). These macroalgae indicate a degraded-eutrophic status of the marsh with excess nutrient inputs, as described for other coastal ecosystems (Teichberg et al., 2010; Le Fur et al., 2018). In our study, nearby marsh aquafarming activities occurring upstream from the estuary can communicate with the rewilded marsh (*c*) through channels and result in high nutrient conditions which could explain observed

macroalgae blooms (Tortajada, 2011). Indeed, at the station *b* channel in September 2018, high DIN concentrations were reported (60.0 µmol L^{-1}; unpublished results). Moreover, shelf waters influenced by terrestrial inputs in winter could also lead to nutrient inputs at the rewilded marsh. Indeed, at the station *F* shelf in winter 2019, NO_3^- ranged between 29 and 107 µmol L^{-1} (Belin et al., 2021). Consequently, these fast-growing macroalgae probably prevented the growth of phytoplankton and seagrasses by nutrient and oxygen competition and light limitation in the water column (Sand-Jensen and Borum, 1991; Le Fur et al., 2018). Simultaneously, in spring and summer, the large water CO_2 undersaturation periods due to the macroalgae autotrophy were maintained through occasional inflows of CO_2 oversaturated channel waters under weak tidal amplitudes. This result is confirmed by significantly higher salinity values in the rewilded marsh waters than in the channel waters during the spring and summer sampling periods (Table 2). On the contrary, macroalgae degradation in autumn probably by microbial remineralization processes (Hill et al., 2015) produced in turn the highest pCO_2 values and the longest oversaturation periods recorded in marsh waters. These heterotrophic processes were confirmed by high NH_4^+ levels (62 µmol L^{-1}; unpublished results) and low DO saturation levels recorded at this period and as described by Newton and Thornber (2013).

Contrarily to the rewilded marsh (*c*), the working marsh (*d*) is managed for salt production in the upstream ponds along the continuum and is directly connected to the estuary (*a*) with no channel in between (Fig. 10). Salt production requires a subtle lock hydraulic management of the marsh depending on the frequency of the coastal water supplies that are mainly controlled by the salt manufacturer and meteorological conditions (rainfall, sunshine and wind) to favour the evaporation process (Paticat, 2007). Therefore, contrary to rewilded marsh, coastal water inflows to the working marsh were performed sparingly with small daily volumes to limit these water mixing effects (i.e. rapid accumulation of large water volumes through rainfall events or

spring tides stop the increase in temperature and salinity in marsh waters; Paticat, 2007). At the working marsh in summer, water pCO_2 values were significantly higher than those measured at the same period at the rewilded marsh but reflected those from the estuary (Table 2). This could also be linked to a lower activity of the primary producers during the summer period dedicated to salt production as confirmed by higher thermal than non-thermal effects on water pCO_2 (Fig. 7). On the other hand, in autumn and winter, lower hydrodynamic conditions due to lock closure (standstill salt farming activity) led to lower water turbidity (< 2 NTU) and nutrient input into the marsh (DIN < 2 µmol L^{-1}; unpublished results) and the growth of seagrasses and phytoplankton produced, in turn, the lowest water pCO_2 values. Overall, in Mediterranean poly-euhaline lagoons, Le Fur et al. (2018) confirmed that nutrient pollution influence the contribution of primary producers from perennial seagrasses in oligotrophic waters to fast-growing macroalgae in eutrophic waters. Similarly, other studies have suggested that the coastal ecosystem management by reducing anthropogenic nutrients could favour blue C ecosystems such as seagrasses and salt marshes (Macreadie et al., 2017, Palacios et al., 2021).

4.4. Metabolism assessment of the sea-land continuums

The tidal estuary (*a*) behaved on average as a yearly CO_2 sink close to the atmospheric equilibrium (Fig. 10), although a significant sink was measured in the spring/summer due to autotrophic activity of phytoplankton in coastal waters. Conversely, over the same meteorological periods, the channel (*b*) was a net annual source from its turbid waters to the atmosphere due to several water CO_2 oversaturation periods (Fig. 10), particularly in winter, characterized by high gas transfer velocities (Table 3). In the Arcachon lagoon, estimated atmospheric CO_2 sources were higher with seasonal means ranging from 0.06 ± 0.04 (winter)

to 0.62 ± 0.66 mmol m^{-2} h^{-1} (summer) with significant diurnal fluctuations (Polsenaere et al., 2022). In this study, eutrophic waters of the rewilded marsh (*c*) behaved as a yearly source of atmospheric CO_2 (Fig. 10), when macroalgae degradation produced strong atmospheric CO_2 effluxes. On the contrary, oligotrophic waters of the working marsh (*d*) behaved as a large yearly CO_2 sink (Fig. 10), favoured by low tidal advection in the absence of salt-farming activities. Within the Duplin River salt marsh-estuary system, both channel and marsh waters degassed CO_2 to the atmosphere and, unlike our stations, the highest and lowest sources were recorded in summer (5.50 and 3.90 mmol m^{-2} h^{-1} from channel and marsh waters, respectively) and in winter (0.70 and 0.60 mmol m^{-2} h^{-1} from channel and marsh waters, respectively), respectively (Wang et al., 2018). Overall, the Duplin system emits more atmospheric CO_2 than the Fier d'Ars system, probably due to its more intense estuarine heterotrophic metabolism.

In autumn, the lack of variations in wind speeds between stations *a* and *b* in 2018 and between stations *c* and *d* in 2019, whereas atmospheric CO_2 exchanges significantly changed, highlighted the predominance of air-water CO_2 gradients in the control of flux directions either as a sink or a source (Table 3). However, at the seasonal scale, turbulence processes measured at the air-water interface played an important role in CO_2 flux variability and magnitude. For instance, at station *a* between spring and summer and at station *b* between winter and summer, wind speed variability produced significant FCO_2 variations although no significant air-water CO_2 gradients were measured (Table 3). Atmospheric exchanges in salt marshes are therefore dependent on the CO_2 saturation state of the water column considering that the wind only acts as a driver of the flux (Polsenaere et al., 2022). Moreover, the methodological calculations and associated differences chosen for the exchange coefficient parameterizations (higher fluxes with RC01 than with W22; Table 3) may produce even more contrasts in the estimated air-water FCO_2 (Cotovicz Jr. et al., 2015; Polsenaere et al., 2022).

By scaling-up and considering stations *a* and *b* together along the continuum, estuarine and channel waters behaved as an annual atmospheric CO_2 source of 7.3 g C m^{-2} yr^{-1}. Whereas, the rewilded marsh emitted 17.5 g C m^{-2} yr^{-1} to the atmosphere, the working marsh absorbed 97.7 g C m^{-2} yr^{-1} from the atmosphere. A larger scale study along three shelf – estuary – tidal wetland continuums on the Atlantic coast of the United States also showed strong spatial variations in atmospheric CO_2 fluxes with uptake to wetland and shelf waters (523.2 ± 148.1 and 10.5 ± 1.8 g C m^{-2} yr^{-1}, respectively) and a source from estuarine waters (110.0 ± 44.5 g C m^{-2} yr^{-1}; Najjar et al., 2018). During our study, contrasting coastal stations were sampled via seasonal 24-h cycles to estimate the air-water CO_2 exchanges. However, longer seasonal measurement periods would be more representative of the strong temporal variability in k_{660}, water pCO_2 and other biogeochemical parameters. At the nearby tidal salt marsh (*e*), emerged for 75% of time during low tides and neap tides, another flux methodology using the atmospheric Eddy Covariance technique was deployed to continuously measure in situ CO_2 fluxes at the ecosystem scale coming from all habitats (aquatic and terrestrial vegetations, mudflats, channels). Over the year 2020, a net uptake of 483 g C m^{-2} yr^{-1} from the atmosphere was measured, indicating a stronger CO_2 sink in tidal marshes than artificial marshes due to higher halophytic plant photosynthesis activity. However, it is also important to study the whole marsh metabolism taking terrestrial and aquatic compartments into account and distinguishing their respective contributions to atmospheric fluxes and the regional C budgets of the associated marshes (Mayen et al., in prep.).

5. Conclusion

Along the continuums, estuarine and channel waters were slightly oversaturated in CO_2 characterized by seasonal compensations of thermal and non-thermal effects whereas, upstream

marsh waters were mostly undersaturated in CO_2 due to stronger biological activity and longer water residence times. At the diurnal/tidal scale, our high-resolution analyses highlighted large water pCO_2 variations in salt marshes, controlled by production and respiration of macrophytes and coastal water inflows. However, anthropogenic management in salt marshes could strongly influence the contribution and turnover of macrophytes and, consequently, the marsh CO_2 sink/source behaviour. Due to eutrophication in the rewilded marsh, development of the fast-growing macroalgae produced an overall net annual atmospheric CO_2 source through their degradation. Our results suggest a winter marsh confinement follow by drying up to limit nutrient inputs and macroalgae development and on the contrary, favour rather slow-growing macrophytes (i.e. seagrasses) which could ultimately contribute to blue C sequestration.

Acknowledgements

We would like to sincerely thank the oyster farmers for their help with taking samples at station *a*, Julien Gernigon from the Lilleau des Niges NNR (LPO) and Brice Collonier from the Loix Ecomuseum for their help and the information given at stations *b*, *c*, *d* and *e*. We are grateful to our colleagues Jean-Michel Chabirand, James Grizon and Philippe Geairon for their help with field sensor deployments and QGIS work. We also thank Quentin Ternon, Gabriel Devique and Jonathan Deborde for their contribution in the field. This paper is a contribution to the Master and Ph.D. thesis of Jérémy Mayen (Ifremer funding), the ANR-PAMPAS project (Agence Nationale de la Recherche « Evolution de l'identité patrimoniale des marais des Pertuis Charentais en réponse à l'aléa de submersion marine », ANR-18-CE32-0006) and the CNRS-INSU LEFE-DYCIDEMAIM project (DYnamique du Carbone aux Interfaces D'Échange des MArais tIdaux teMpérés). The English language was edited by Sara Mullin (Ph.D.).

Adam, P., 2019. Salt Marsh Restoration, in: Coastal Wetlands. Elsevier, pp. 817–861. https://doi.org/10.1016/B978-0-444-63893-9.00023-X

Aminot A, Kerouel R (2004). Hydrologie des écosystèmes marins. Paramètres et analyses. Ed. Ifremer

Amorocho, J., DeVries, J.J., 1980. A new evaluation of the wind stress coefficient over water surfaces. J. Geophys. Res. 85, 433. https://doi.org/10.1029/JC085iC01p00433

Artigas, F., Shin, J.Y., Hobble, C., Marti-Donati, A., Schäfer, K.V.R., Pechmann, I., 2015. Long term carbon storage potential and CO_2 sink strength of a restored salt marsh in New Jersey. Agricultural and Forest Meteorology 200, 313–321. https://doi.org/10.1016/j.agrformet.2014.09.012

Aufdenkampe, A.K., Mayorga, E., Raymond, P.A., Melack, J.M., Doney, S.C., Alin, S.R., Aalto, R.E., Yoo, K., 2011. Riverine coupling of biogeochemical cycles between land, oceans, and atmosphere. Frontiers in Ecology and the Environment 9, 53–60. https://doi.org/10.1890/100014

Bade, D.L., 2009. Gas Exchange at the Air–Water Interface, in: Encyclopedia of Inland Waters. Elsevier, pp. 70–78. https://doi.org/10.1016/B978-012370626-3.00213-1

Baldocchi, D.D., Hincks, B.B., Meyers, T.P., 1988. Measuring Biosphere-Atmosphere Exchanges of Biologically Related Gases with Micrometeorological Methods. Ecology 69, 1331–1340. https://doi.org/10.2307/1941631

Bauer, J.E., Cai, W.-J., Raymond, P.A., Bianchi, T.S., Hopkinson, C.S., Regnier, P.A.G., 2013. The changing carbon cycle of the coastal ocean. Nature 504, 61–70. https://doi.org/10.1038/nature12857

Bel Hassen, M., 2001. Spatial and Temporal Variability in Nutrients and Suspended Material Processing in the Fier d'Ars Bay (France). Estuarine, Coastal and Shelf Science 52, 457–469. https://doi.org/10.1006/ecss.2000.0754

Belin, C., Soudant, D., Amzil, Z., 2021. Three decades of data on phytoplankton and phycotoxins on the French coast: Lessons from REPHY and REPHYTOX. Harmful Algae 102, 101733. https://doi.org/10.1016/j.hal.2019.101733

Berg, P., Delgard, M.L., Polsenaere, P., McGlathery, K.J., Doney, S.C., Berger, A.C., 2019. Dynamics of benthic metabolism, O_2, and pCO_2 in a temperate seagrass meadow. Limnol Oceanogr 64, 2586–2604. https://doi.org/10.1002/lno.11236

Borges, A.V., Frankignoulle, M., 1999. Daily and seasonal variations of the partial pressure of CO_2 in surface seawater along Belgian and southern Dutch coastal areas. Journal of Marine Systems 19, 251–266. https://doi.org/10.1016/S0924-7963(98)00093-1

Borges, A.V., 2003. Atmospheric CO_2 flux from mangrove surrounding waters. Geophys. Res. Lett. 30, 1558. https://doi.org/10.1029/2003GL017143

Borges, A.V., Delille, B., Frankignoulle, M., 2005. Budgeting sinks and sources of CO_2 in the coastal ocean: Diversity of ecosystems counts: COASTAL CO_2 SINKS AND SOURCES. Geophys. Res. Lett. 32, LI4601 https://doi.org/10.1029/2005GL023053

Borges, A.V., Abril, G., 2011. Carbon Dioxide and Methane Dynamics in Estuaries, in: Treatise on Estuarine and Coastal Science. Elsevier, pp. 119–161. https://doi.org/10.1016/B978-0-12-374711-2.00504-0

Bozec, Y., Merlivat, L., Baudoux, A.-C., Beaumont, L., Blain, S., Bucciarelli, E., Danguy, T., Grossteffan, E., Guillot, A., Guillou, J., Répécaud, M., Tréguer, P., 2011. Diurnal to inter-annual dynamics of pCO_2 recorded by a CARIOCA sensor in a temperate coastal ecosystem (2003–2009). Marine Chemistry 126, 13–26. https://doi.org/10.1016/j.marchem.2011.03.003

Burgos, M., Ortega, T., Forja, J., 2018. Carbon Dioxide and Methane Dynamics in Three Coastal Systems of Cadiz Bay (SW Spain). Estuaries and Coasts 41, 1069–1088. https://doi.org/10.1007/s12237-017-0330-2

Cai, W.-J., 2011. Estuarine and Coastal Ocean Carbon Paradox: CO_2 Sinks or Sites of Terrestrial Carbon Incineration? Annu. Rev. Mar. Sci. 3, 123–145. https://doi.org/10.1146/annurev-marine-120709-142723

Champion E, Gernigon J, Lemesle J-C, Terrisse J, Maisonhaute S (2012) 3ème Plan de gestion 2013-2017 de la réserve naturelle nationale de Lilleau des Niges

Chmura, G.L., Anisfeld, S.C., Cahoon, D.R., Lynch, J.C., 2003. Global carbon sequestration in tidal, saline wetland soils. Global Biogeochem. Cycles 17, 1111 https://doi.org/10.1029/2002GB001917

Cloern, J.E., 1987. Turbidity as a control on phytoplankton biomass and productivity in estuaries. Continental Shelf Research, Dynamics of Turbid Coastal Environments 7, 1367–1381. https://doi.org/10.1016/0278-4343(87)90042-2

Cloern, J.E., Foster, S.Q., Kleckner, A.E., 2014. Phytoplankton primary production in the world's estuarine-coastal ecosystems. Biogeosciences 11, 2477–2501. https://doi.org/10.5194/bg-11-2477-2014

Coignot, E., P. Polsenaere, P. Soletchnik, O. Le Moine, P. Souchu, E. Joyeux, Y. Le Roy, J.-P. Guéret, L. Froud, R. Gallais, E. Chourré, and L. Chaigneau. 2020. Variabilité spatio-temporelle des nutriments et du carbone et flux associés le long d'un continuum terrestre-aquatique tempéré (Marais poitevin – Baie de l'Aiguillon – Pertuis Breton). Rapport final (suivi 2017-2018) - Projet Aiguillon (2016–2020). 111pp. https://archimer.ifremer.fr/doc/00618/73003/.

Cole, J.J., Prairie, Y.T., Caraco, N.F., McDowell, W.H., Tranvik, L.J., Striegl, R.G., Duarte, C.M., Kortelainen, P., Downing, J.A., Middelburg, J.J., Melack, J., 2007. Plumbing the Global Carbon Cycle: Integrating Inland Waters into the Terrestrial Carbon Budget. Ecosystems 10, 172–185. https://doi.org/10.1007/s10021-006-9013-8

Cotovicz Jr., L.C., Knoppers, B.A., Brandini, N., Costa Santos, S.J., Abril, G., 2015. A strong CO_2 sink enhanced by eutrophication in a tropical coastal embayment (Guanabara Bay, Rio de Janeiro, Brazil). Biogeosciences 12, 6125–6146. https://doi.org/10.5194/bg-12-6125-2015

Crosswell, J.R., Anderson, I.C., Stanhope, J.W., Dam, B.V., Brush, M.J., Ensign, S., Piehler, M.F., McKee, B., Bost, M., Paerl, H.W., 2017. Carbon budget of a shallow, lagoonal estuary: Transformations and source-sink dynamics along the river-estuary-ocean continuum. Limnology and Oceanography 62, S29–S45. https://doi.org/10.1002/lno.10631

Dai, M., Lu, Z., Zhai, W., Chen, B., Cao, Z., Zhou, K., Cai, W.-J., Chenc, C.-T.A., 2009. Diurnal variations of surface seawater pCO_2 in contrasting coastal environments. Limnol. Oceanogr. 54, 735–745. https://doi.org/10.4319/lo.2009.54.3.0735

Dai, M., Su, J., Zhao, Y., Hofmann, E.E., Cao, Z., Cai, W.-J., Gan, J., Lacroix, F., Laruelle, G.G., Meng, F., Müller, J.D., Regnier, P.A.G., Wang, G., Wang, Z., 2022. Carbon Fluxes in the Coastal Ocean: Synthesis, Boundary Processes, and Future Trends. Annu. Rev. Earth Planet. Sci. 50, 593–626. https://doi.org/10.1146/annurev-earth-032320-090746

Deegan, L.A., Johnson, D.S., Warren, R.S., Peterson, B.J., Fleeger, J.W., Fagherazzi, S., Wollheim, W.M., 2012. Coastal eutrophication as a driver of salt marsh loss. Nature 490, 388–392. https://doi.org/10.1038/nature11533

Dickson, A.G., and F.J. Millero. 1987. A comparison of the equilibrium constants for the dissociation of carbonic acid in seawater media. *Deep-Sea Research* 34: 1733‑1743.

Dickson, A.G. 1990. Standard potential of the reaction: AgCl(s) + 1⁄2H_2(g) = Ag(s) + HCl(aq), and the standard acidity constant of the ion HSO_4 – in synthetic sea water from 273.15 to 318.15 K. Journal of Chemical Thermodynamics 22: 113–127.

Duarte, C.M., Cebrián, J., 1996. The fate of marine autotrophic production. Limnol. Oceanogr. 41, 1758–1766. https://doi.org/10.4319/lo.1996.41.8.1758

Dürr, H.H., Laruelle, G.G., van Kempen, C.M., Slomp, C.P., Meybeck, M., Middelkoop, H., 2011. Worldwide Typology of Nearshore Coastal Systems: Defining the Estuarine Filter of River Inputs to the Oceans. Estuaries and Coasts 34, 441–458. https://doi.org/10.1007/s12237-011-9381-y

Forbrich, I., Giblin, A.E., 2015. Marsh- atmosphere CO_2 exchange in a New England salt marsh. J. Geophys. Res. Biogeosci. 120, 1825–1838. https://doi.org/10.1002/2015JG003044

Frankignoulle, M., Abril, G., Borges, A., Bourge, I., Canon, C., Delille, B., Libert, E., Théate, J.-M., 1998. Carbon Dioxide Emission from European Estuaries. Science, New Series 282, 434–436.

Gattuso, J.-P., Frankignoulle, M., Wollast, R., 1998. CARBON AND CARBONATE METABOLISM IN COASTAL AQUATIC ECOSYSTEMS. Annu. Rev. Ecol. Syst. 29, 405–434. https://doi.org/10.1146/annurev.ecolsys.29.1.405

Gu, J., Luo, M., Zhang, X., Christakos, G., Agusti, S., Duarte, C.M., Wu, J., 2018. Losses of salt marsh in China: Trends, threats and management. Estuarine, Coastal and Shelf Science 214, 98–109. https://doi.org/10.1016/j.ecss.2018.09.015

Guarini, J.-M., Gros, P., Blanchard, G., Richard, P., Fillon, A., 2004. Benthic contribution to pelagic microalgal communities in two semi-enclosed, European-type littoral ecosystems (Marennes-Oléron Bay and Aiguillon Bay, France). Journal of Sea Research 52, 241–258. https://doi.org/10.1016/j.seares.2004.04.003

Guarini, J.-M., Sari, N., Moritz, C., 2008. Modelling the dynamics of the microalgal biomass in semi-enclosed shallow-water ecosystems. Ecological Modelling 211, 267–278. https://doi.org/10.1016/j.ecolmodel.2007.09.011

Harrell, F.E., 2015. Regression Modeling Strategies: With Applications to Linear Models, Logistic and Ordinal Regression, and Survival Analysis, Springer Series in Statistics. Springer International Publishing, Cham. https://doi.org/10.1007/978-3-319-19425-7

Hill, R., Bellgrove, A., Macreadie, P.I., Petrou, K., Beardall, J., Steven, A., Ralph, P.J., 2015. Can macroalgae contribute to blue carbon? An Australian perspective: Can macroalgae contribute to blue carbon? Limnol. Oceanogr. 60, 1689–1706. https://doi.org/10.1002/lno.10128

Jähne, B., Münnich, K.O., Bösinger, R., Dutzi, A., Huber, W., Libner, P., 1987. On the parameters influencing air-water gas exchange. J. Geophys. Res. 92, 1937. https://doi.org/10.1029/JC092iC02p01937

Jiang, L.-Q., Cai, W.-J., Wang, Y., 2008. A comparative study of carbon dioxide degassing in river- and marine-dominated estuaries. Limnol. Oceanogr. 53, 2603–2615. https://doi.org/10.4319/lo.2008.53.6.2603

Krause-Jensen, D., Duarte, C.M., 2016. Substantial role of macroalgae in marine carbon sequestration. Nature Geosci 9, 737–742. https://doi.org/10.1038/ngeo2790

Le Fur, I., De Wit, R., Plus, M., Oheix, J., Simier, M., Ouisse, V., 2018. Submerged benthic macrophytes in Mediterranean lagoons: distribution patterns in relation to water chemistry and depth. Hydrobiologia 808, 175–200. https://doi.org/10.1007/s10750-017-3421-y

Lê, S., Josse, J., Husson, F., 2008. FactoMineR: An *R* Package for Multivariate Analysis. J. Stat. Soft. 25. https://doi.org/10.18637/jss.v025.i01

Lee, K., Kim, T.-W., Byrne, R.H., Millero, F.J., Feely, R.A., Liu, Y.-M., 2010. The universal ratio of boron to chlorinity for the North Pacific and North Atlantic oceans. Geochimica et Cosmochimica Acta 74, 1801–1811. https://doi.org/10.1016/j.gca.2009.12.027

Lewis, E. and D. Wallace. 1998. Program developed for CO_2 system calculations. Carbon dioxide information analysis center. Oak Ridge National Laboratory.

Macreadie, P.I., Nielsen, D.A., Kelleway, J.J., Atwood, T.B., Seymour, J.R., Petrou, K., Connolly, R.M., Thomson, A.C., Trevathan-Tackett, S.M., Ralph, P.J., 2017. Can we manage coastal ecosystems to sequester more blue carbon? 8. https://doi.org/10.1002/fee.1484

Mcleod, E., Chmura, G.L., Bouillon, S., Salm, R., Björk, M., Duarte, C.M., Lovelock, C.E., Schlesinger, W.H., Silliman, B.R., 2011. A blueprint for blue carbon: toward an improved understanding of the role of vegetated coastal habitats in sequestering CO_2. Frontiers in Ecology and the Environment 9, 552–560. https://doi.org/10.1890/110004

Mehrbach, C., Culberson, C.H., Hawley, J.E., Pytkowicz, R.M., 1973. Measurement of the Apparent Dissociation Constants of Carbonic Acid in Seawater at Atmospheric Pressure. Limnology and Oceanography 18, 897–907.

Najjar, R.G., Herrmann, M., Alexander, R., Boyer, E.W., Burdige, D.J., Butman, D., Cai, W. - J., Canuel, E.A., Chen, R.F., Friedrichs, M.A.M., Feagin, R.A., Griffith, P.C., Hinson, A.L., Holmquist, J.R., Hu, X., Kemp, W.M., Kroeger, K.D., Mannino, A., McCallister, S.L., McGillis, W.R., Mulholland, M.R., Pilskaln, C.H., Salisbury, J., Signorini, S.R., St- Laurent, P., Tian, H., Tzortziou, M., Vlahos, P., Wang, Z.A., Zimmerman, R.C., 2018. Carbon Budget of Tidal Wetlands, Estuaries, and Shelf Waters of Eastern North America. Global Biogeochem. Cycles 32, 389–416. https://doi.org/10.1002/2017GB005790

Newton, C., Thornber, C., 2013. Ecological Impacts of Macroalgal Blooms on Salt Marsh Communities. Estuaries and Coasts 36, 365–376. https://doi.org/10.1007/s12237-012-9565-0

Palacios, M.M., Trevathan-Tackett, S.M., Malerba, M.E., Macreadie, P.I., 2021. Effects of a nutrient enrichment pulse on blue carbon ecosystems. Marine Pollution Bulletin 165, 112024. https://doi.org/10.1016/j.marpolbul.2021.112024

Paticat, F., 2007. Flux et usages de l'eau de mer dans les marais salés endigués Charentais: Cas du marais salé endigué de l'île de Ré (Thèse). Université Nantes.

Polsenaere, P., Lamaud, E., Lafon, V., Bonnefond, J.-M., Bretel, P., Delille, B., Deborde, J., Loustau, D., Abril, G., 2012. Spatial and temporal CO_2 exchanges measured by Eddy Covariance over a temperate intertidal flat and their relationships to net ecosystem production. Biogeosciences 9, 249–268. https://doi.org/10.5194/bg-9-249-2012

Polsenaere, P., Deborde, J., Detandt, G., Vidal, L.O., Pérez, M.A.P., Marieu, V., Abril, G., 2013. Thermal enhancement of gas transfer velocity of CO_2 in an Amazon floodplain lake revealed by eddy covariance measurements: GAS TRANSFER VELOCITY IN AN AMAZON LAKE. Geophys. Res. Lett. 40, 1734–1740. https://doi.org/10.1002/grl.50291

Polsenaere, P., Delille, B., Poirier, D., Charbonnier, C., Deborde, J., Mouret, A., Abril, G., 2022. Seasonal, Diurnal, and Tidal Variations of Dissolved Inorganic Carbon and pCO_2 in Surface Waters of a Temperate Coastal Lagoon (Arcachon, SW France). Estuaries and Coasts. https://doi.org/10.1007/s12237-022-01121-6

Raven, J., 2018. Blue carbon: past, present and future, with emphasis on macroalgae. Biol. Lett. 14, 20180336. https://doi.org/10.1098/rsbl.2018.0336

Raymond, P.A., Cole, J.J., 2001. Gas Exchange in Rivers and Estuaries: Choosing a Gas Transfer Velocity. Estuaries 24, 312. https://doi.org/10.2307/1352954

REPHY – French Observation and Monitoring program for Phytoplankton and Hydrology in coastal waters, 2021. REPHY dataset - French Observation and Monitoring program for Phytoplankton and Hydrology in coastal waters. Metropolitan data. SEANOE. https://doi.org/10.17882/47248

Ribas-Ribas, M., Gómez-Parra, A., Forja, J.M., 2011. Air–sea CO_2 fluxes in the north-eastern shelf of the Gulf of Cádiz (southwest Iberian Peninsula). Marine Chemistry 123, 56–66. https://doi.org/10.1016/j.marchem.2010.09.005

Sand-Jensen, K., Borum, J., 1991. Interactions among phytoplankton, periphyton, and macrophytes in temperate freshwaters and estuaries. Aquatic Botany 41, 137–175. https://doi.org/10.1016/0304-3770(91)90042-4

Savelli, R., Bertin, X., Orvain, F., Gernez, P., Dale, A., Coulombier, T., Pineau, P., Lachaussée, N., Polsenaere, P., Dupuy, C., Le Fouest, V., 2019. Impact of Chronic and Massive Resuspension Mechanisms on the Microphytobenthos Dynamics in a Temperate Intertidal Mudflat. J. Geophys. Res. Biogeosci. 124, 3752–3777. https://doi.org/10.1029/2019JG005369

Schäfer, K.V.R., Tripathee, R., Artigas, F., Morin, T.H., Bohrer, G., 2014. Carbon dioxide fluxes of an urban tidal marsh in the Hudson-Raritan estuary: Carbon dioxide fluxes of a wetland. J. Geophys. Res. Biogeosci. 119, 2065–2081. https://doi.org/10.1002/2014JG002703

Soletchnik, P., Polsenaere, P., Le Moine, O., Guesdon, S., Béchemin, C., 2015. Relations entre apports terrigènes et conchyliculture dans les Pertuis Charentais. :pp. 1–53. http:// archimer.ifremer.fr/doc/00248/35964/.

Stanisière, J.Y., Dumas, F., Plus, M., Maurer, D., Robert, S., 2006. Caractérisation des composantes hydrodynamiques d'un système côtier semi-fermé: Le Bassin de Marennes-Oléron. :pp. 1–112. http://archimer.ifremer.fr/doc/00000/2353/.

Takahashi, T., Sutherland, S.C., Sweeney, C., Poisson, A., Metzl, N., Tilbrook, B., Bates, N., Wanninkhof, R., Feely, R.A., Sabine, C., Olafsson, J., Nojiri, Y., 2002. Global sea–air CO_2 flux based on climatological surface ocean pCO_2, and seasonal biological and temperature effects. Deep Sea Research Part II: Topical Studies in Oceanography 49, 1601–1622. https://doi.org/10.1016/S0967-0645(02)00003-6

Teichberg, M., Fox, S.E., Olsen, Y.S., Valiela, I., Martinetto, P., Iribarne, O., Muto, E.Y., Petti, M.A.V., Corbisier, T.N., Soto- Jiménez, M., Páez- Osuna, F., Castro, P., Freitas, H., Zitelli, A., Cardinaletti, M., Tagliapietra, D., 2010. Eutrophication and macroalgal blooms in temperate and tropical coastal waters: nutrient enrichment experiments with *Ulva* spp. Global Change Biology 16, 2624–2637. https://doi.org/10.1111/j.1365-2486.2009.02108.x

Tobias, C., Neubauer, S.C., 2019. Salt Marsh Biogeochemistry—An Overview, in: Coastal Wetlands. Elsevier, pp. 539–596. https://doi.org/10.1016/B978-0-444-63893-9.00016-2

Tortajada, S., 2011. De l'étude du fonctionnement des réseaux trophiques planctoniques des marais de Charente Maritime vers la recherche d'indicateurs (Thèse). Université La Rochelle.

Tortajada, S., David, V., Brahmia, A., Dupuy, C., Laniesse, T., Parinet, B., Pouget, F., Rousseau, F., Simon-Bouhet, B., Robin, F.-X., 2011. Variability of fresh- and salt-water marshes characteristics on the west coast of France: A spatio-temporal assessment. Water Research 45, 4152–4168. https://doi.org/10.1016/j.watres.2011.05.024

Van Dam, B., Polsenaere, P., Barreras- Apodaca, A., Lopes, C., Sanchez- Mejia, Z., Tokoro, T., Kuwae, T., Loza, L.G., Rutgersson, A., Fourqurean, J., Thomas, H., 2021. Global Trends in Air- Water CO_2 Exchange Over Seagrass Meadows Revealed by Atmospheric Eddy Covariance. Global Biogeochem Cycles 35. https://doi.org/10.1029/2020GB006848

Vandermeirsch, F., 2012. ÉTAT PHYSIQUE ET CHIMIQUE Caractéristiques physiques.

Wang, S.R., Di Iorio, D., Cai, W., Hopkinson, C.S., 2018. Inorganic carbon and oxygen dynamics in a marsh- dominated estuary. Limnol. Oceanogr. 63, 47–71. https://doi.org/10.1002/lno.10614

Wang, Z.A., Cai, W.-J., 2004. Carbon dioxide degassing and inorganic carbon export from a marsh-dominated estuary (the Duplin River): A marsh CO_2 pump. Limnol. Oceanogr. 49, 341–354. https://doi.org/10.4319/lo.2004.49.2.0341

Wang, Z.A., Kroeger, K.D., Ganju, N.K., Gonneea, M.E., Chu, S.N., 2016. Intertidal salt marshes as an important source of inorganic carbon to the coastal ocean. Limnol. Oceanogr. 61, 1916–1931. https://doi.org/10.1002/lno.10347

Wanninkhof, R., Pierrot, D., Sullivan, K., Mears, P., Barbero, L., 2022. Comparison of discrete and underway CO_2 measurements: Inferences on the temperature dependence of the fugacity of CO_2 in seawater. Marine Chemistry 247, 104178. https://doi.org/10.1016/j.marchem.2022.104178

Wei, T., Simko, V., 2017. R package "corrplot": Visualization of a Correlation Matrix. https://github.com/taiyun/corrplot

Weiss, R.F., 1974. Carbon dioxide in water and seawater: the solubility of a non-ideal gas. Marine Chemistry 2, 203–215. https://doi.org/10.1016/0304-4203(74)90015-2

Yates, K.K., Dufore, C., Smiley, N., Jackson, C., Halley, R.B., 2007. Diurnal variation of oxygen and carbonate system parameters in Tampa Bay and Florida Bay. Marine Chemistry 104, 110–124. https://doi.org/10.1016/j.marchem.2006.12.008

Fig. 1. The Fier d'Ars estuary (Ré Island, French Atlantic coast) and locations of the four studied stations along aquatic continuums: tidal estuary at station *a*, channel at station *b*, rewilded artificial salt marsh at station *c* (in green) and working artificial salt marsh at station *d* (in blue). The dyke (in red) delimits terrestrial and maritime areas. The locks in the two studied artificial marshes are represented within the two map expansions. An atmospheric Eddy Covariance station was deployed at station *e* on the tidal salt marsh downstream from the dyke. Station *F* is located in the centre of the Breton Sound continental shelf; station *a* is located at the entry of the estuary; stations *b*, *c* and *e* are within the National Natural Reserve to the west of the estuary; station *d* to the east of the estuary is within a salt-farm.

Fig. 2. Principal Component Analysis (PCA) of the biogeochemical parameters measured at each season along the studied aquatic continuums (stations *a*, *b*, *c* and *d*). The PCA is based on temperature (Temp), salinity, turbidity, dissolved oxygen concentration (DO), dissolved oxygen saturation level (DO-sat.) and pCO_2 mean values for each 24-h cycle. Stations *a*, *b*, *c* and *d* are represented in red, brown, green and blue, respectively. The additional station *F* is represented in light blue. Win: Winter; Spr: Spring; Sum: Summer; Aut: Autumn.

Fig. 3. Temporal variations at station *a* (tidal estuary) of water temperature (°C), salinity, DO saturation level (DO-sat., %), turbidity (NTU), pCO_2, $NpCO_2$ (pCO_2 variations related to non-temperature effects, ppmv) and $TpCO_2$ (pCO_2 variations related to temperature physical effects, ppmv) during each 24-h cycle from winter 2018 to autumn 2018. Parameters were autonomously measured once per minute by in situ probes. Water heights (H, m) were retrieved from the SHOM station (9 km away; Fig. 1). Grey areas correspond to night-time periods. Vertical dotted lines correspond to high tides. Horizontal dotted lines correspond to the CO_2 atmospheric concentration (411 ppm; NOAA 2018). Each graduation of the x-axis corresponds to one hour.

Fig. 4. Temporal variations at station *b* (channel) of water temperature (°C), salinity, DO saturation level (DO-sat., %), turbidity (NTU), pCO_2, $NpCO_2$ and $TpCO_2$ (ppmv) during each 24-h cycle from winter 2018 to autumn 2018. See the Fig. 3 caption for more details.

Fig. 5. Temporal variations at station *c* (rewilded artificial salt marsh) of water temperature (°C), salinity, DO saturation level (DO-sat., %), turbidity (NTU), pCO_2, $NpCO_2$ and $TpCO_2$ (ppmv) and *in situ* Chl *a* (µg L^{-1}) during each 24-h cycle from spring 2019 to winter 2020. Vertical dotted lines correspond to coastal water inflows to the marsh during incoming tide. Horizontal dotted lines correspond to the atmospheric CO_2 concentration simultaneously measured (i) by the Eddy Covariance (station *e*) during the summer and winter cycles and (ii) by NOAA during the spring and autumn cycles. *In situ* Chl *a* values are represented by black crosses (Chl $a_{measured}$); no water samples could be taken in spring 2019. See the Fig. 3 caption for more details.

Fig. 6. Temporal variations at station *d* (working artificial salt marsh) of water temperature (°C), salinity, DO saturation level (DO-sat., %), turbidity (NTU), pCO_2, $NpCO_2$ and $TpCO_2$ (ppmv) and *in situ* Chl *a* (µg L^{-1}) during each 24-h cycle from summer 2019 to winter 2020. Chl *a* values in green were derived from the C3-fluorometer every 10 min. (Chl $a_{estimated}$). See the Fig. 3 caption for more details.

Fig. 7. Derived temperature-normalized pCO_2 (seasonal $NpCO_2$, blue curves with empty blue dots) and thermally forced pCO_2 (seasonal $TpCO_2$, pink curves with empty pink dots) at the seasonal scale at stations *F*, *a*, *b*, *c* and *d*. Seasonal means of water temperature (in red dotted lines) and pCO_2 (red curves with filled red dots) are also represented. Horizontal dotted lines correspond to CO_2 atmospheric concentration (411 ppm; NOAA 2018).

Fig. 8. Diurnal/tidal correlation plots of temperature vs. salinity and water pCO_2 vs. salinity at stations *b* and *c* for each season. Only significant R^2 (slopes significantly different from zero; n = 1441; $p < 0.05$) are showed. HT/D: high tide day; LT/D: low tide day; HT/N: high tide night; LT/N: low tide night. At station *c*, HT periods correspond to coastal water inflows to the marsh. Note that the temperature and salinity ranges across the seasons are not the same. Horizontal dotted lines correspond to the atmospheric CO_2 concentration.

Fig. 9. Seasonal and spatial variations in estimated CO_2 fluxes (FCO_2, in mmol m^{-2} h^{-1}) at the water-atmosphere interface at stations *F*, *a*, *b*, *c* and *d*. The means and associated standard deviations over each 24-h cycle are shown. k_{660} and FCO_2 estimations were calculated according to the R22 parametrization. FCO_2 values at stations *a* and *b* are only given for high tide periods.

Fig. 10. CO_2 budget over the two aquatic sea - land continuums: (1) continental shelf - estuary - channel - rewilded artificial salt marsh and (2) continental shelf - estuary - working artificial salt marsh. Annual means (± SD) and ranges (min - max) of water pCO_2 (ppmv) and air-water FCO_2 (mmol m^{-2} h^{-1}) are showed. The picture of station *c* in spring 2019 (© P. Polsenaere) allows to visualize the macroalgae bloom.

Fig. 1.

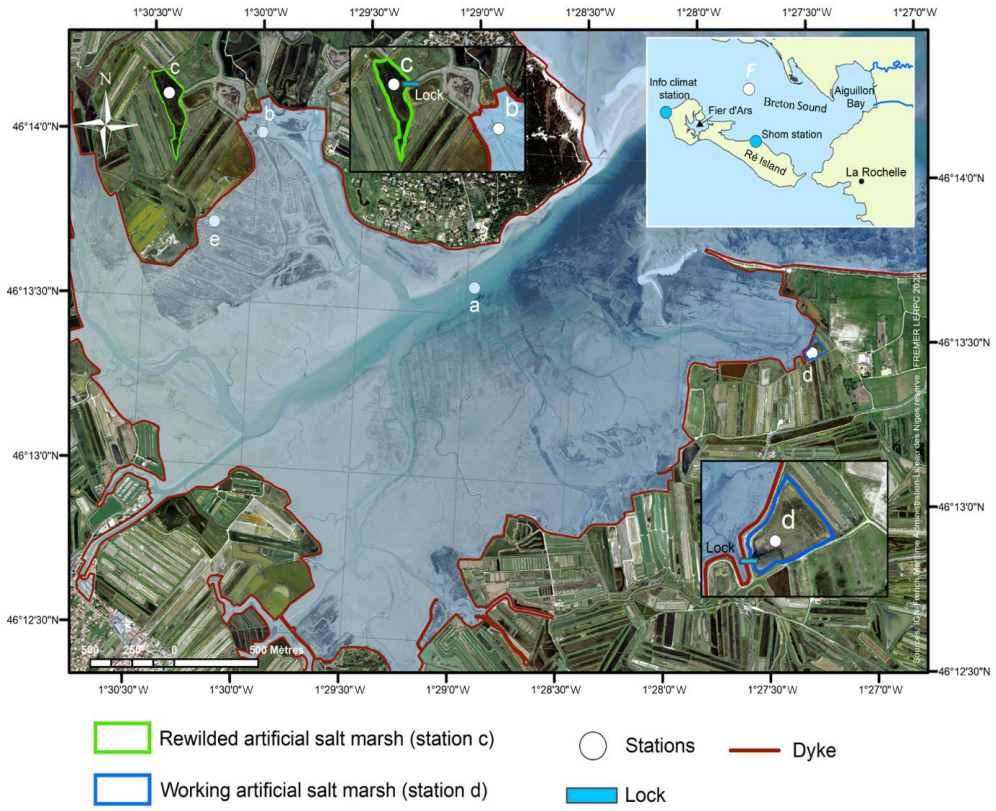

Fig. 2.

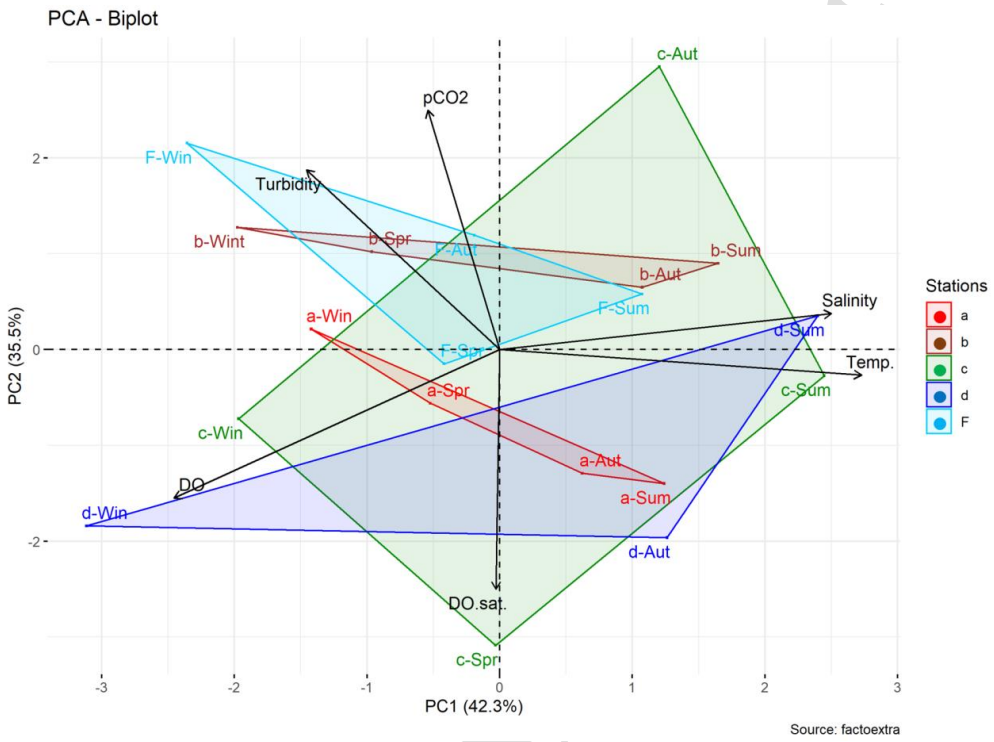

Fig. 3.

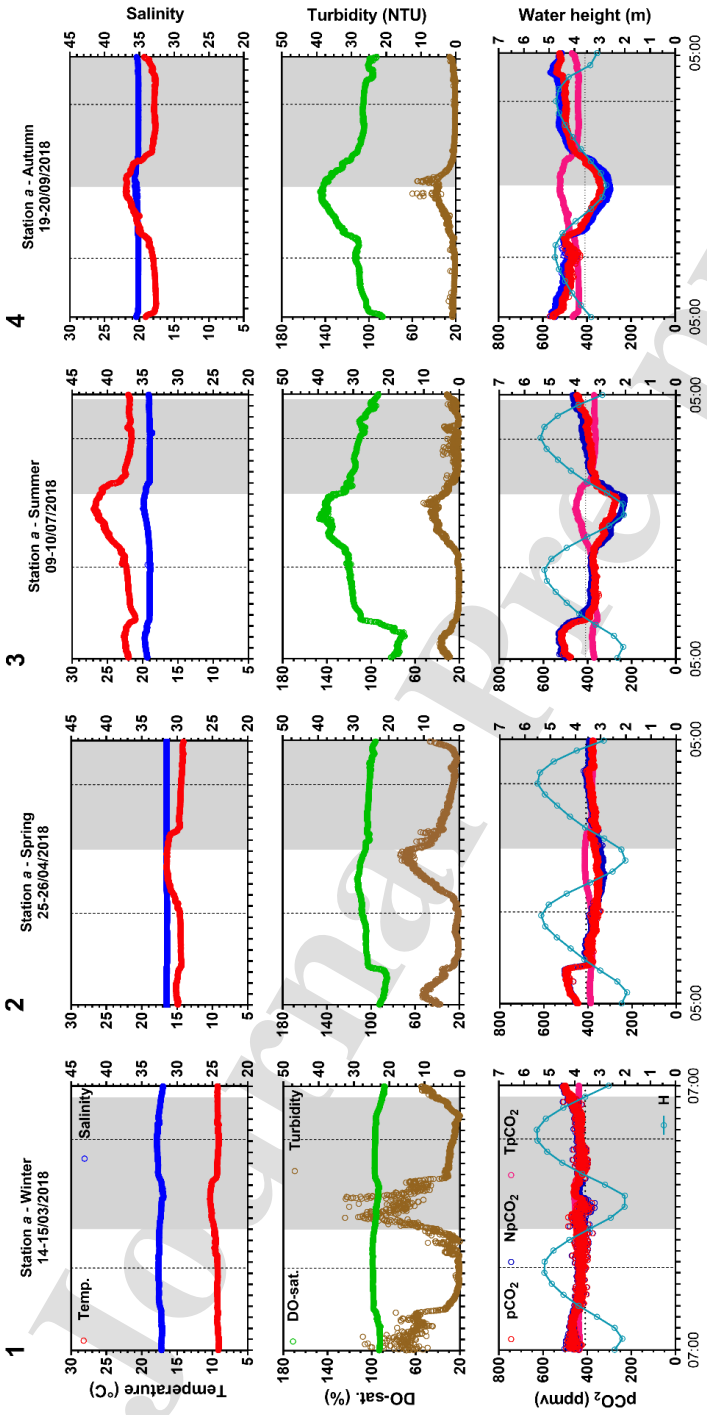

Fig. 4.

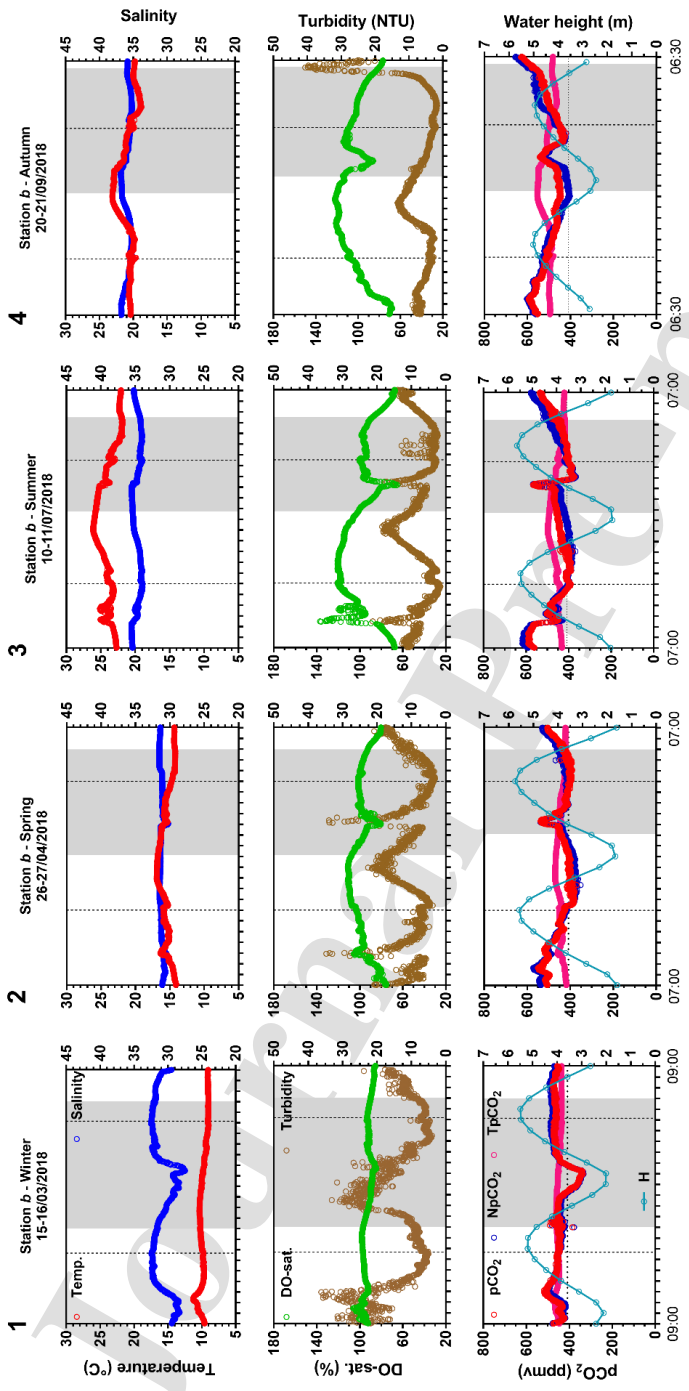

Fig. 5.

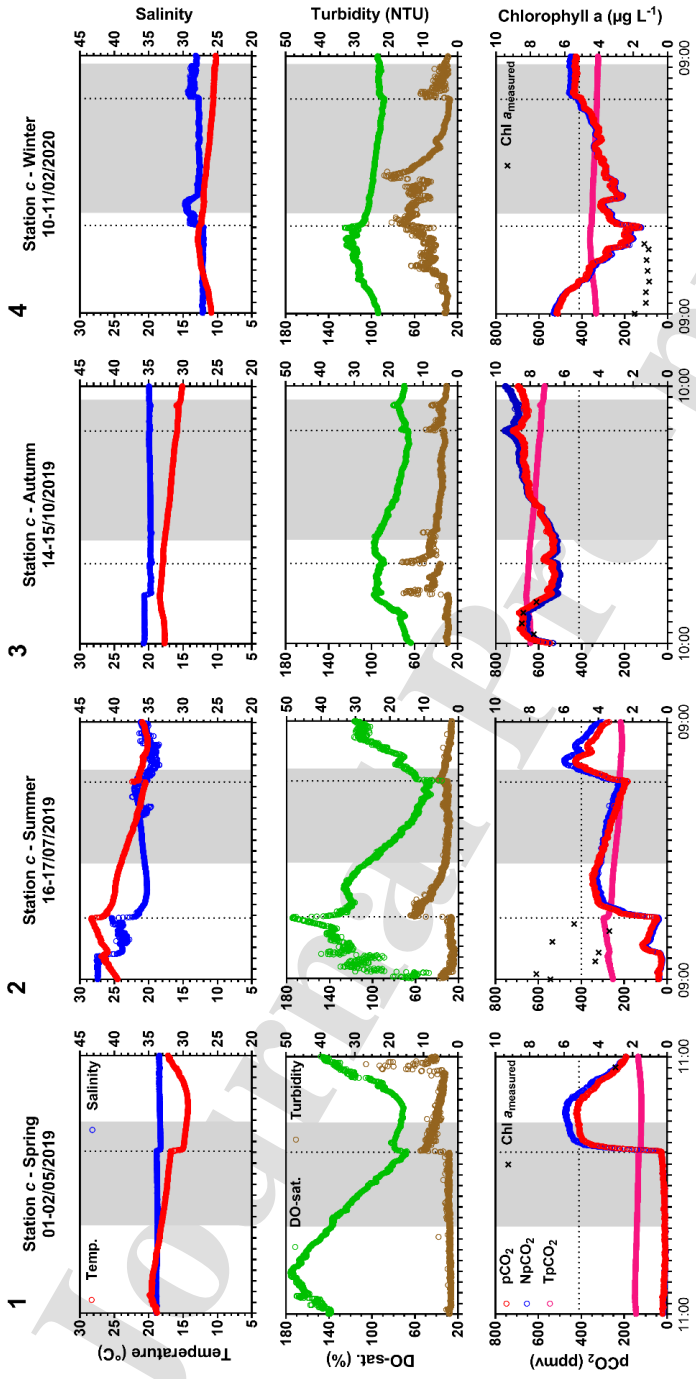

Fig. 6

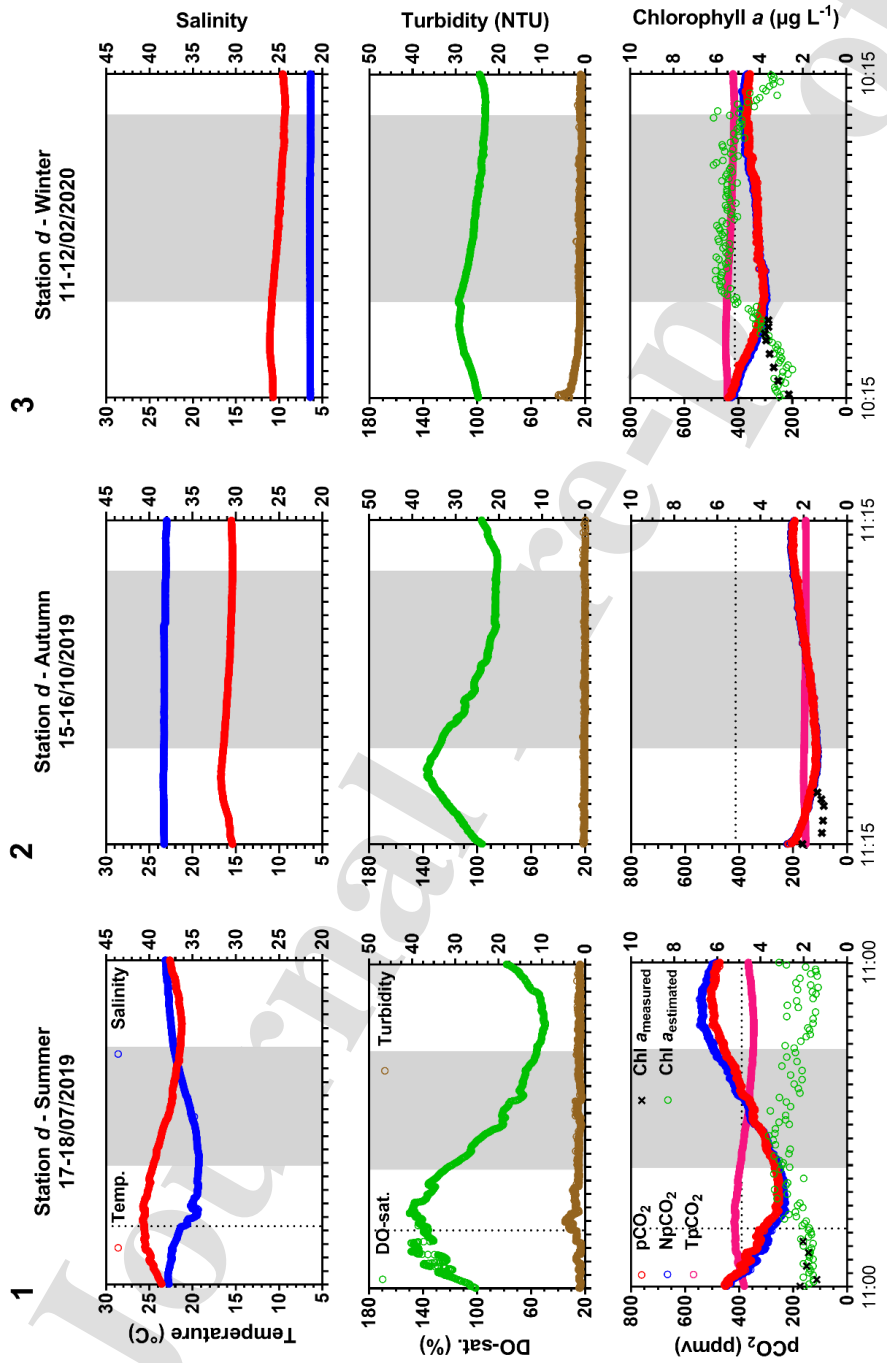

Fig. 7.

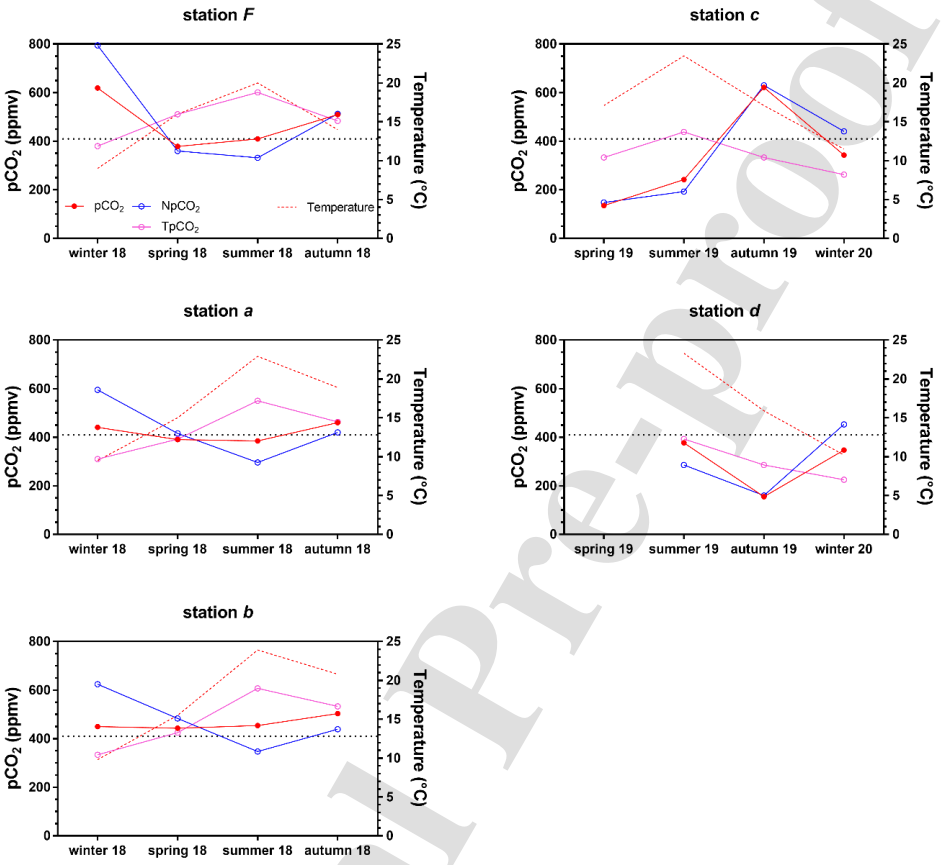

Fig. 8.

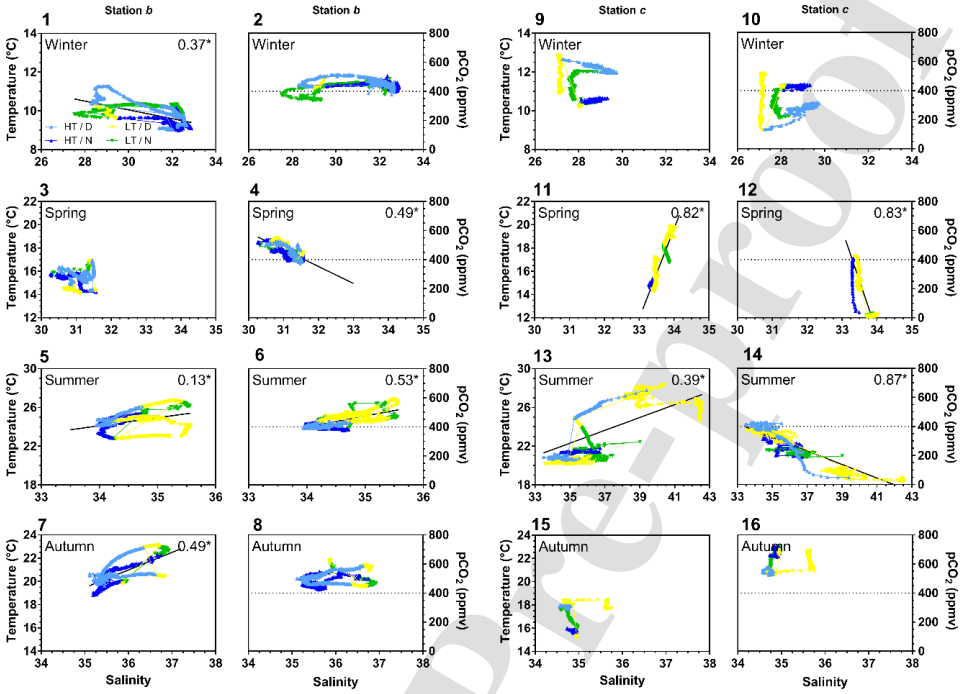

Fig. 9.

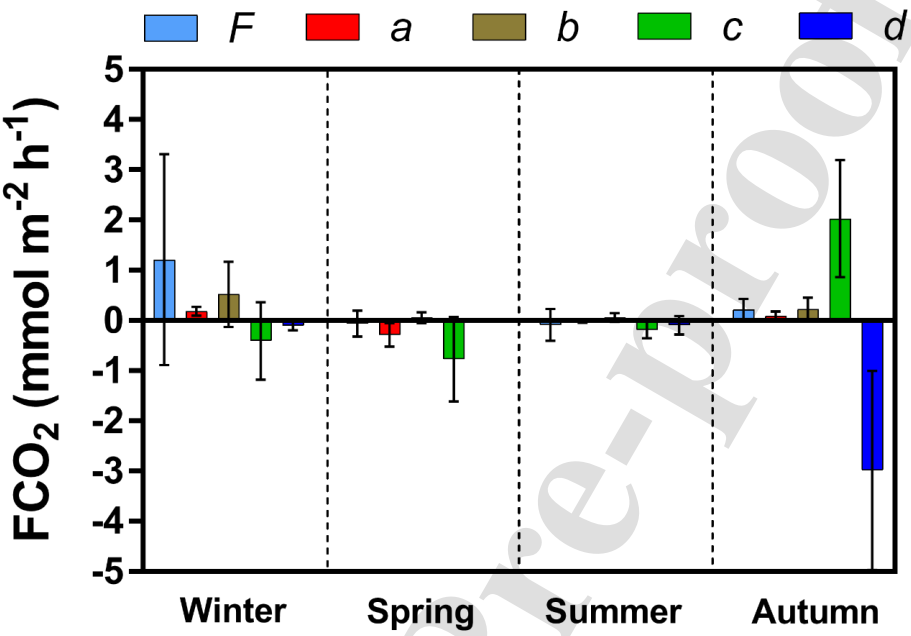

Fig. 10.

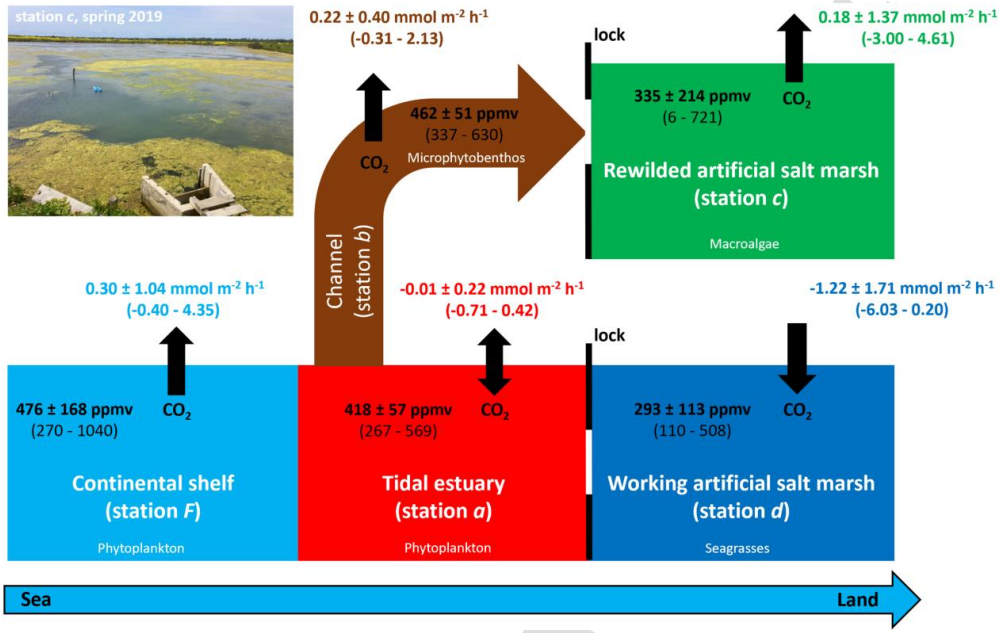

Table 1: Meteorological conditions (air temperature in °C and cumulative precipitation in mm) obtained from the "Infoclimat" station on Ré Island (Fig. 1; https://www.infoclimat.fr) at the monthly and annual scales over our measurement periods in 2018, 2019 and 2020 in bold compared to the reference period (1990-2020).

Year	Season	Month	Mean air temperature (°C)	Difference with the reference period (°C)	Cumulative precipitation (mm)	Difference with the reference period (mm)
2018	**Winter**	March	**9.1**	-0.7	**127**	+70
	Spring	April	**13.4**	+1.4	**58**	-3
	Summer	July	**22.2**	+1.7	**59**	+19
	Autumn	September	**19.0**	+1.0	**9**	-51
		Annual	**14.3**	+0.8	**786**	+32
2019	**Spring**	April	**11.9**	-0.1	**57**	-4
	Summer	July	**22.5**	+2.0	**33**	-7
	Autumn	October	**15.8**	+1.1	**117**	+33
		Annual	**14.1**	+0.6	**827**	+73
2020	**Winter**	February	**10.4**	+3.1	**68**	+12

Table 2: Seasonal means (± SD) and ranges (min - max) of temperature (°C), salinity, DO (µmol L^{-1}), pH (NBS scale) and pCO_2 (ppmv) values measured (i) once every two weeks in 2018 at station *F* (Coignot et al., 2020) and (ii) during each 24-h cycle from 2018 to 2020 at stations *a*, *b*, *c* and *d* in this study.

		Temperature (°C)	**Salinity**	**DO (µmol L^{-1})**	**pH (NBS)**	**pCO_2 (ppmv)**
Winter 2018	*F*	**9.1 ± 1.3** (7.5 - 10.6)	**31.4 ± 1.8** (28.9 - 33.0)	**269.6 ± 29.7** (225.0 - 285.3)	**8.04 ± 0.17** (7.79 - 8.17)	**619 ± 285** (415 - 1040)
March 2018	*a*	**9.5 ± 0.4** (9.1 - 10.4)	**32.5 ± 0.2** (31.9 - 32.9)	**278.7 ± 7.7** (257.2 - 288.8)	-	**441 ± 21** (377 - 510)
March 2018	*b*	**9.8 ± 0.5** (9.0 - 11.3)	**31.0 ± 1.4** (27.5 - 32.5)	**269.7 ± 9.3** (251.6 - 307.5)	-	**450 ± 33** (337 - 518)
February 2020	*c*	**11.5 ± 0.7** (10.2 - 12.9)	**27.8 ± 0.7** (27.0 - 29.7)	**287.5 ± 22.0** (256.9 - 350.0)	**8.20 ± 0.14** (7.94 - 8.53)	**343 ± 87** (130 - 519)
February 2020	*d*	**10.2 ± 0.6** (9.2 - 11.1)	**21.4 ± 0.0** (21.3 - 21.5)	**314.5 ± 15.9** (293.1 - 343.8)	**8.27 ± 0.04** (8.16 - 8.32)	**347 ± 30** (302 - 438)
Spring 2018	*F*	**16.0 ± 2.5** (13.2 - 19.1)	**32.4 ± 1.5** (30.8 - 34.2)	**270.0 ± 28.5** (245.3 - 308.2)	**8.23 ± 0.09** (8.11 - 8.33)	**379 ± 89** (279 - 495)
April 2018	*a*	**15.0 ± 0.7** (14.1 - 16.5)	**31.5 ± 0.0** (31.4 - 31.5)	**265.8 ± 16.4** (221.9 - 285.3)	**8.17 ± 0.03** (8.09 - 8.21)	**390 ± 40** (342 - 505)
April 2018	*b*	**15.5 ± 0.9** (14.1 - 16.9)	**31.2 ± 0.3** (30.3 - 31.6)	**252.2 ± 20.1** (200.3 - 279.4)	**8.05 ± 0.02** (7.98 - 8.09)	**443 ± 44** (371 - 551)
May 2019	*c*	**17.1 ± 1.8** (14.3 - 19.9)	**33.7 ± 0.2** (33.3 - 34.0)	**287.5 ± 78.4** (168.4 - 415.0)	**8.78 ± 0.43** (8.12 - 9.23)	**135 ± 165** (6 - 425)
-	*d*	-	-	-	-	-
Summer 2018	*F*	**19.9 ± 1.5** (18.2 - 21.7)	**34.6 ± 0.6** (34.0 - 35.2)	**235.6 ± 22.3** (204.4 - 253.1)	**8.20 ± 0.12** (8.05 - 8.34)	**410 ± 130** (270 - 572)
July 2018	*a*	**22.9 ± 1.6** (21.0 - 26.9)	**34.2 ± 0.3** (33.6 - 34.9)	**249.4 ± 35.9** (153.4 - 306.6)	**8.22 ± 0.07** (8.12 - 8.39)	**385 ± 60** (267 - 522)
July 2018	*b*	**23.9 ± 1.3** (21.9 - 26.1)	**34.7 ± 0.5** (33.9 - 35.6)	**211.8 ± 33.9** (139.7 - 291.9)	**8.02 ± 0.05** (7.89 - 8.12)	**454 ± 55** (374 - 590)
July 2019	*c*	**23.5 ± 2.5** (20.1 - 28.4)	**36.8 ± 2.3** (33.5 - 42.6)	**206.8 ± 58.5** (76.9 - 339.7)	**8.31 ± 0.23** (8.01 - 8.94)	**242 ± 116** (25 - 430)
July 2019	*d*	**23.3 ± 1.6** (21.2 - 28.1)	**35.8 ± 1.4** (33.3 - 38.1)	**202.4 ± 70.4** (108.8 - 314.4)	**7.97 ± 0.09** (7.84 - 8.11)	**377 ± 85** (250 - 508)
Autumn 2018	*F*	**14.7 ± 3.2** (10.3 - 17.5)	**34.3 ± 2.1** (30.6 - 35.4)	**249.1 ± 23.5** (225.0 - 284.4)	**8.09 ± 0.06** (8.04 - 8.18)	**510 ± 70** (403 - 580)
September 2018	*a*	**18.9 ± 1.5** (17.6 - 22.0)	**35.2 ± 0.1** (35.1 - 35.7)	**267.4 ± 25.9** (204.7 - 323.4)	**7.98 ± 0.07** (7.90 - 8.16)	**460 ± 58** (334 - 569)
September 2018	*b*	**20.8 ± 1.2** (18.8 - 23.1)	**35.9 ± 0.5** (35.1 - 36.9)	**232.1 ± 30.3** (153.8 - 275.3)	**7.84 ± 0.05** (7.74 - 7.94)	**503 ± 46** (422 - 630)
October 2019	*c*	**17.1 ± 0.9** (15.1 - 18.5)	**35.0 ± 0.3** (34.6 - 35.7)	**194.3 ± 24.4** (152.2 - 236.9)	**7.82 ± 0.04** (7.74 - 7.91)	**622 ± 57** (522 - 721)
October 2019	*d*	**15.9 ± 0.4** (15.4 - 16.8)	**38.2 ± 0.1** (38.0 - 38.4)	**255.8 ± 39.9** (210.6 - 331.9)	**8.17 ± 0.07** (8.07 - 8.28)	**155 ± 30** (110 - 218)

Table 3: Seasonal means (± SD) and ranges (min - max) of wind speed (km h^{-1}), gas transfer velocity (k_{660}, cm h^{-1}) and estimated water-atmosphere CO_2 flux (FCO_2, mmol m^{-2} h^{-1}) values measured (i) once every two weeks in 2018 at station *F* (Coignot et al., 2020) and (ii) during each 24-h cycle from 2018 to 2020 at stations *a*, *b*, *c* and *d* in the present study. Air CO_2 concentrations used for FCO_2 calculations are: 408 ppm (stations *a*, *b* and *F* in 2018), 411 ppm (station *c* in spring 2019), 413 ppm (stations *c* and *d* in autumn 2019), 400 ppm (stations *c* and *d* in summer 2019) and 403 ppm (stations *c* and *d* in winter 2020; see M&M sections).

		Wind speed (km h^{-1})	k_{660} (cm h^{-1})		FCO_2 (mmol m^{-2} h^{-1})	
			W22	RC01	W22	RC01
Winter 2018	*F*	**19 ± 10** (7 - 29)	**7.45 ± 6.30** (0.91 - 14.24)	**11.29 ± 8.83** (2.79 - 21.62)	**1.21 ± 2.10** (0.01 - 4.35)	**1.85 ± 3.18** (0.02 - 6.60)
March 2018	*a*	**29 ± 4** (22 - 37)	**14.93 ± 4.04** (8.63 - 24.68)	**24.75 ± 9.92** (12.08 - 52.53)	**0.18 ± 0.09** (0.09 - 0.42)	**0.28 ± 0.14** (0.13 - 0.69)
March 2018	*b*	**32 ± 12** (13 - 54)	**21.39 ± 15.99** (3.02 - 54.68)	**66.17 ± 87.62** (5.06 - 285.40)	**0.52 ± 0.65** (-0.31 - 2.13)	**1.91 ± 3.45** (-0.46 - 11.11)
February 2020	*c*	**27 ± 5** (16 - 34)	**23.17 ± 10.28** (6.93 - 39.66)	**30.36 ± 13.28** (9.21 - 50.44)	**-0.40 ± 0.77** (-2.02 - 0.94)	**-0.68 ± 1.31** (-3.58 - 1.58)
February 2020	*d*	**15 ± 5** (4 - 24)	**6.92 ± 3.17** (2.15 - 14.23)	**9.46 ± 4.34** (2.96 - 19.78)	**-0.10 ± 0.09** (-0.31 - 0.09)	**-0.15 ± 0.13** (-0.41 - 0.13)
Spring 2018	*F*	**15 ± 20** (11 - 20)	**5.35 ± 3.44** (2.41 - 9.32)	**7.78 ± 3.91** (4.43 - 12.40)	**-0.06 ± 0.26** (-0.40 - 0.22)	**-0.09 ± 0.34** (-0.54 - 0.30)
April 2018	*a*	**33 ± 7** (24 - 43)	**24.01 ± 9.56** (11.85 - 38.49)	**51.64 ± 32.90** (16.94 - 108.70)	**-0.29 ± 0.23** (-0.71 - 0.11)	**-0.66 ± 0.65** (-1.81 - 0.18)
April 2018	*b*	**14 ± 5** (4 - 22)	**4.62 ± 2.96** (0.35 - 10.44)	**7.23 ± 3.46** (2.55 - 13.62)	**0.05 ± 0.11** (-0.06 - 0.33)	**0.08 ± 0.15** (-0.08 - 0.46)
May 2020	*c*	**18 ± 7** (6 - 31)	**8.99 ± 6.31** (0.86 - 22.99)	**12.86 ± 9.09** (3.17 - 37.67)	**-0.77 ± 0.84** (-3.00 - 0.03)	**-1.21 ± 1.30** (-5.09 - 0.04)
-	*d*	-	-	-	-	-
Summer 2018	*F*	**20 ± 12** (4 - 32)	**12.85 ± 10.75** (0.36 - 24.50)	**20.41 ± 17.10** (2.56 - 40.89)	**-0.09 ± 0.31** (-0.34 - 0.31)	**-0.08 ± 0.49** (-0.50 - 0.51)
July 2018	*a*	**11 ± 3** (6 - 17)	**3.50 ± 1.97** (0.89 - 7.21)	**6.35 ± 2.13** (3.55 - 10.40)	**-0.02 ± 0.03** (-0.08 - 0.08)	**-0.03 ± 0.06** (-0.14 - 0.16)
July 2018	*b*	**18 ± 7** (7 - 30)	**9.69 ± 6.37** (1.29 - 23.89)	**14.66 ± 9.28** (4.15 - 39.18)	**0.06 ± 0.08** (-0.07 - 0.22)	**0.09 ± 0.13** (-0.11 - 0.37)
July 2019	*c*	**13 ± 4** (4 - 19)	**4.56 ± 2.59** (0.43 - 9.46)	**7.59 ± 2.92** (3.16 - 13.32)	**-0.19 ± 0.17** (-0.70 - 0.01)	**-0.33 ± 0.24** (-1.01 - 0.02)
July 2019	*d*	**15 ± 6** (2 - 23)	**7.12 ± 4.60** (0.11 - 14.77)	**10.77 ± 5.72** (2.41 - 20.96)	**-0.09 ± 0.18** (-0.43 - 0.20)	**-0.12 ± 0.27** (-0.60 - 0.29)
Autumn 2018	*F*	**17 ± 5** (11 - 22)	**6.37 ± 4.09** (2.25 - 10.83)	**9.01 ± 4.98** (4.08 - 14.46)	**0.21 ± 0.22** (-0.02 - 0.56)	**0.30 ± 0.29** (-0.02 - 0.75)
September 2018	*a*	**11 ± 6** (4 - 20)	**3.55 ± 3.27** (0.36 - 8.98)	**6.21 ± 3.66** (2.65 - 12.53)	**0.09 ± 0.09** (0.01 - 0.30)	**0.15 ± 0.11** (0.01 - 0.41)
September 2018	*b*	**17 ± 6** (11 - 32)	**7.32 ± 5.46** (2.90 - 24.27)	**9.46 ± 7.91** (4.02 - 42.48)	**0.22 ± 0.23** (0.07 - 1.00)	**0.28 ± 0.33** (0.05 - 1.75)
October 2019	*c*	**35 ± 8** (20 - 48)	**27.39 ± 11.52** (9.01 - 48.79)	**63.79 ± 42.95** (12.58 - 179.80)	**2.03 ± 1.17** (0.61 - 4.61)	**4.86 ± 4.22** (0.85 - 16.98)
October 2019	*d*	**42 ± 7** (31 - 54)	**38.22 ± 12.55** (20.54 - 62.36)	**122.80 ± 84.13** (34.76 - 325.40)	**-3.43 ± 1.09** (-6.03 - -1.79)	**-10.91 ± 7.35** (-31.46 - -3.03)

Table 4. Stepwise multilinear regression analyses to test the contribution of physicochemical variables on water pCO_2 variations through the percentage of explained variance (adjusted R^2). Each selected multilinear model ($p < 0.001$, $n = 1441$) had the highest adjusted R^2 value with all variables explaining at least 5% of the pCO_2 variation. In bold is indicated the parameter explaining at least 50% of the pCO_2 variation. Input variables: DO-sat. (dissolved oxygen saturation level), T (water temperature), S (salinity) and TU (turbidity). The statistic (F) and adjusted R^2 (adj. R^2) are given.

			Equations	**F**	**adj. R^2**
Winter	March 2018	*a*	pCO_2 = 2227.7 - 3.7 **DO-sat.** - 19.9 T - 38.2 S	1004	67.7%
	March 2018	*b*	pCO_2 = -373.8 + 21.1 S + 0.8 TU + 15.9 T	377	43.9%
	February 2020	*c*	pCO_2 = 1460.5 - 158.3 **T** + 7.0 DO-sat.	1180	62.1%
	February 2020	*d*	pCO_2 = 446.6 - 10.8 DO-sat. + 99.1 T	4723	86.8%
Spring	April 2018	*a*	pCO_2 = 949.8 - 5.5 **DO-sat.**	8255	85.2%
	April 2018	*b*	pCO_2 = 2542.0 - 4.0 **DO-sat.** - 61.7 S + 14.2 T	1923	80.0%
	May 2019	*c*	pCO_2 = 21777.7 - 640.8 **S** - 0.6 DO-sat.	3668	83.6%
	-	*d*	-		-
Summer	July 2018	*a*	pCO_2 = 747.2 - 3.2 **DO-sat.**	30524	95.5%
	July 2018	*b*	pCO_2 = -2440.0 + 100.8 **S** - 25.4 T	3330	82.7%
	July 2019	*c*	pCO_2 = 1961.5 - 46.7 **S**	9401	86.8%
	July 2019	*d*	pCO_2 = -961.8 + 40.1 **S** - 1.2 DO-sat.	47983	98.5%
Autumn	September 2018	*a*	pCO_2 = 923.1 - 4.1 **DO-sat.**	34905	96.4%
	September 2018	*b*	pCO_2 = 782.0 - 2.8 **DO-sat.** + 1.1 TU	3066	81.0%
	October 2019	*c*	pCO_2 = 1009.3 - 4.9 **DO-sat.**	8831	86.0%
	October 2019	*d*	pCO_2 = 1932.7 + 1.6 **DO-sat.** - 122.7 T	3253	81.9%

CRediT author statement

Jérémy Mayen: Methodology, Software, Validation, Formal analysis, Investigation, Writing - Original - Draft, Writing - Review & Editing. **Pierre Polsenaere:** Conceptualization, Methodology, Software, Validation, Formal analysis, Investigation, Ressources, Writing - Review & Editing, Supervision, Project Administration, Funding acquisition. **Aurore Regaudie De Gioux:** Writing - Review & Editing, Supervision, Funding acquisition. **Christine Dupuy:** Validation, Writing - Review & Editing. **Marie Vagner:** Writing - Review & Editing, Funding acquisition. **Jean-Christophe Lemesle:** Resources. **Benoit Poitevin:** Resources. **Philippe Souchu:** Validation, Writing - Review & Editing, Supervision, Funding acquisition.

Declaration of interests

☒ The authors declare that they have no known competing financial interests or personal relationships that could have appeared to influence the work reported in this paper.

☐ The authors declare the following financial interests/personal relationships which may be considered as potential competing interests: